Velocity shear instability and plasma billows at the Earth's magnetic boundary

2012 J. Phys.: Conf. Ser. 370 012003

(http://iopscience.iop.org/1742-6596/370/1/012003)

Journal of Physics: Conference Series **370** (2012) 012003 doi:10.1088/1742-6596/370/1/012003

Velocity shear instability and plasma billows at the Earth's magnetic boundary

F T Gratton[1,2], G Gnavi[1-3], C J Farrugia[4], L Bilbao[1-3] and R Torbert[4]

[1]Instituto de Física del Plasma, Consejo Nacional de Investigaciones Científicas y Técnicas y Universidad de Buenos Aires, Buenos Aires, Argentina
[2]Departamento de Física, Facultad de Ciencias Fisicomatemáticas e Ingeniería, Pontificia Universidad Católica Argentina, Buenos Aires, Argentina
[3]Departamento de Física, Facultad de Ciencias Exactas y Naturales, Universidad de Buenos Aires, Buenos Aires, Argentina
[4]Space Science Center, University of New Hampshire, Durham, NH, 03824, USA

E-mail: fgratton@arnet.com.ar

Abstract. The Kelvin-Helmoltz instability (KH) with formation of vortices appears in a wide variety of terrestrial, interplanetary, and astrophysical contexts. We study a series of iterated rolled-up coherent plasma structures (15) that flow in the equatorial Earth's boundary layer (BL), observed on October 24, 2001. The data were recorded during a 1.5 hour-long Wind crossing of the BL at the dawn magnetospheric flank, tailward of the terminator ($X\approx$-13 R_E). The interplanetary magnetic field (IMF) was radially directed, almost antiparallel to the magnetosheath (MS) flow. This configuration is expected to be adverse to the KH instability because of the collinearity of field and flow, and the high compressibility of the MS. We analyze the BL stability with compressible MHD theory using continuous profiles for the physical quantities. Upstream, at near Earth sites, we input parameters derived from an exact MHD solution for collinear flows. Further downtail at Wind position we input measured parameters. The BL is found KH unstable in spite of unfavorable features of the external flow. On the experimental side, the passage of vortices is inferred from the presence of low density - hot plasma being accelerated to speeds higher than that of the contiguous MS. It is further supported by the peculiar correlation of relative motions (in the bulk velocity frame): cold-dense plasma drifts sunward, while hot-tenuous plasma moves tailward. This event differs from many other studies that reported BL vortices under strongly northward IMF orientations. This is a case of KH vortices observed under an almost radial IMF, with implicit significance for the more common Parker's spiral fields, and the problem of plasma entry in the magnetosphere.

1. Introduction

1.1. Foreword

The first part of the (plenary conference) paper is an introduction to the Kelvin-Helmholtz (KH) instability in terrestrial plasmas. The importance of KH phenomena relies on the enhancement of momentum, energy, and eventually the mass transport they cause. While the presence of this instability is pervasive in terrestrial, interplanetary, and cosmic scenarios, here we limit the study to

the Earth´s magnetosphere. The physics that we learn via *in situ* observations can also provide lessons for remote scenarios of the universe that cannot be explored directly.

The "*the flow-driven*" instability and its effects occur throughout the solar system. We call to mind the presence of KH in our atmosphere, and at the bottom of the oceans. The phenomenon has been observed on planets and at the Sun itself. The first part describes several aspects of KH in the magnetosphere of Earth based on our past investigations which offer promising prospects for further studies. A summary review of magnetohydrodynamic (MHD) properties of the instability is included, to support the second part that contains a new research on a peculiar KH event, observed on October 24, 2001 by the spacecraft Wind.

The topics treated in the paper are the following. 1) Notes on manifestations of velocity gradient instabilities in the solar system. 2) Basic notions on the KH instability, and elements of a MHD treatment. 3) Aspects of Kelvin-Helmholtz research in the space environment of Earth with potential for deeper studies. 4) An unusual event of magnetopause instability with almost collinear magnetic field and flow. 5) The experimental evidence of KH vortices in the boundary layer during the Wind traversal of October 24, 2001.

1.2. The ubiquitous Kelvin-Helmholtz instability

Vortex formation, breaking of sea waves, and billows in atmosphere clouds are part of our common experience. There are frequent observations of Kelvin-Helmholtz vortices in our atmosphere. Their importance for meteorology has been appreciated since the second part of the XIX century. The KH mechanism is present in the billowy wake of wind blowing over a mountain ridge (see photos in Tritton's textbook, and also NASA [1]). Kelvin-Helmholtz clouds resemble the breaking of waves in the ocean. Evaporation and condensation patterns help the visualization of the capped tops and cloudless troughs of the billows. In the following we use the words vortex and billow as synonimous (To our knowledge, the first use of billow in a MP context was made in [67]).

The vortices generated by the KH effect appear in lee waves downstream of an island of the southern Pacific Ocean. Observed by Landsat (1999) [2] from above, the Alexander Selkirk island is a striking example. Rising steeply, the island's highest point is 1600 m above sea level. As wind-driven clouds encounter this obstacle, they flow around it to form large, spinning eddies. KH due to velocity gradients appears also inside hurricanes. Kelvin–Helmholtz billows were photographed (from an aircraft at an altitude of 4500 m) in the eye-wall of Hurricane Erin (at 18:15 UTC, 10 Sep 2001 [3]).

A classic example of a KH phenomenon is the formation, growth, and break of water waves in wind - sea interaction. Kelvin-Helmholtz vortices are also found deep under water, in oceanic floors. Non-linear waves breaking on the slope of submarine mountains of the Atlantic ocean, 1100 km south of the Azores were recently reported (2011 [4]). A line of temperature probes at a depth of 500 m recorded the passage of the structures, with wavelengths ≈ 75 m, and periods ≈ 50 s.

Proceeding to the planets, KH structures in the Saturn atmosphere were observed by the Cassini probe from 5.9 million km, on October 9, 2004 (NASA [5]). The KH vortices are due to the interaction of two belts of Saturn's atmosphere. This phenomenon is estimated to be frequent in the gaseous giant planets because of the alternated jets and the temperature differences of atmospheric strips and belts. Another case of an atmospheric vortex is Jupiter's giant red spot, which was observed to last for at least 300 years.

The Cassini satellite also observed a plasma vortex in Saturn's dayside magnetosphere [6]. The probe encountered the vortex on 13 December 2004 as it was travelling toward the planet. The spacecraft crossed the magnetopause three times, before being immersed in the low-latitude boundary layer (BL). During the transition between the boundary layer and the magnetosphere proper, the spacecraft observed a deflected boundary layer plasma, and a twisted magnetic field topology. The data are interpreted as an encounter with a vortex on the inner edge of the boundary layer, an interface susceptible to the growth of the KH instability due to its low magnetic shear. We return to this point in section 4.

In space plasmas magnetic effects add to the complexity, and the variety of KH phenomena. The Solar Dynamics Observatory (SDO), presently the most recent and advanced spacecraft devoted to solar studies, provides detailed views at high resolution of plasma filaments that rise from Sun's spots, of plasma arcades sustained by magnetic fields, and solar eruptions. On the subject of the Kelvin–Helmholtz instability at the Sun itself see Foullon et al., 2011 [7]. During the readjustments of flow and field of the high solar atmosphere, following a strong commotion produced by a coronal mass ejection (CME) KH phenomena were also recorded by SDO, 2011 [7].

The solar wind is a continuous expansion of the coronal plasma that fills interplanetary space. It reaches supersonic speeds already close to the Sun. The planets constitute occasional obstacles that generate local shock waves in the solar wind flow. Magnetized planets, like the Earth, have a bow shock, after which the plasma flow is subsonic for some stretch, and have also a magnetosphere. The magnetosphere is dominated by the magnetic field of the planet. A current sheet separates the shocked plasma in the magnetosheath from the magnetosphere. At the interface between the magnetosheath

and the magnetosphere – the magnetopause – the KH instability may occur.

A general comprehensive study, theory and observations, of the physics of the Sun´s atmosphere and the interplanetary plasma is available in the monograph edited by Russel and Kivelson (1995) [8]. During the outward flow of solar wind there are several occasions where the KH instability may occur. For instance, recently the Messenger mission published magnetic records that are interpreted as the formation of KH vortices at Mercury [9].

Moreover, the solar wind has a bimodal structure. Fast solar wind streams, from 700 – 800 km/s and more, originate in coronal holes. Slow solar winds 300 – 400 km/s come mainly from Sun's equatorial belt. At the interface between plasmas moving with different speeds (for example, [10]) the KH instability can grow.

1.3. Terrestrial magnetosphere.

The possibility of significant perturbations of the Earth's magnetopause caused by the KH instabiliy has a long history, and a large literature. It was first suggested by Dungey (1954) [11], who was also the first to hypothesize the reconnection of magnetic field lines in the frontside under IMF south, and beyond the polar cusps during periods of IMF north (Dungey (1961) [12]). The transition between magnetosheath and magnetosphere where velocity and density gradients appear is the MP boundary layer (BL).

During several decades the possibility of energy and momentum transfer from the solar wind to the magnetosphere by KH effects has been considered in a number of theoretical and observational papers. We recall some significant examples, Axford and Hines (1961) [13], Southwood (1968) [14], Sonnerup (1980) [15], Hones et al., (1981) [16], Ogilvie y Fitzenreiter (1989) [17], among many others, and draw the reader's attention to the references in reviews of the subject. For instance, Belmont y Chanteur (1989) [18], Miura (1995) [19], Fitzenreiter y Ogilvie (1995) [20], Kivelson y Chen (1995) [21], Farrugia et al. (2001) [22], *inter alia*.

The evidence for the presence of the instability is either direct, from data analysis of *in situ* records of spacecraft crossing the MP, or indirect, by inference from measurements of ground magnetometer chains at high geographical latitudes. Examples of the former are the studies of multiple boundary layer (BL) crossings by a spacecraft, consistent with large amplitude surface waves, likely of KH origin, moving downtail, Lepping and Burlaga [23], Seon et al. [24]. Regarding the latter method, it is now generally accepted (see [8]) that the KH instability causes pulsed oscillations of the geomagnetic field in the Pc5 range (Samson and Rostoker [25]) with periods in the range 150-600 s (e.g., [26])) Seon et al. [24], for instance, quote periods 120-240 s attributed to observed KH waves.

The knowledge of the KH instability and its evolution is complemented by numerical simulations that provide data analysis with important interpretive concepts and schematics. MHD computational studies of the KH in the MP context started with Miura (1984) [27]. The plausibility of MHD for space physics was argued, and explained by E. N. Parker in the 1960s. Since then MHD has been a powerful help to study the solar wind and its interaction with the terrestrial magnetosphere. Steady

90progress can be appraised in a set of reviews of the topic (for instance:[18], [19], [21]), and several recent research papers, Fairfield and Otto (2000) [28], Nykyri and Otto (2001; 2003) [29], Smets et al. (2002) [30], Hasegawa et al. (2004; 2009) [31], Gratton et al. (2006, 2009, 2011) [32], Bilbao 2009 [32], Nakamura et al., (2006; 2008) [33]), Hwang et al., (2011) [34], amongst many.

1.4. The cold dense plasma sheet

The transport process through the MP that produces the so called cold dense plasma sheet (CDPS), located around the central equatorial plane of the magnetospheric tail is at the focus of a debate since the discovery of the phenomenon (Fujimoto and Teresawa (1994) [35]). The CDPS is a plasma at a lower temperature, and higher density than the ordinary hot and tenuous magnetospheric plasma. Space scientists investigate possible mechanisms by which plasma enters the magnetosphere under different conditions of geomagnetic configuration, solar wind, and solar cycle. Because of the frequent observation *in situ* of the CDPS during periods of northward IMF the subject engages the attention of the magnetospheric community.

During periods of northward IMF the KH instability is an important mechanism of momentum and energy transfer from the solar wind to the magnetosphere. Recent studies (Otto and Fairfield (2000) [36]) maintain that the non-linear stage of the KH instability, accompanied by large vortices that roll-up plasma of the magnetosheath and mingle it with magnetospheric plasma in the MP flanks, generate inside the big eddies favorable conditions to plasma entry during north IMF phases (see also [28], [29], [30], [31], [32], [33]). The transfer processes inside the large eddies include diffusion and/or, under certain conditions, convection and stretching of magnetic field lines.The latter progress until thin current sheets are formed, which may form localized, small-scale, magnetic reconnections, with the possibility of mass entry. We report observations of current sheets formed in a row of vortices of the magnetospheric BL in sections 4 – 5.

Other investigators support the hypothesis that reconnection of magnetic field lines beyond the polar cups is the main mechanism of entrance of mass during periods of IMF north. A simultaneous reconnection in the vicinity of both, northern and southern, cusps generate flux tubes full of magnetosheath plasma that penetrating in the magnetosphere would sink gradually inside, while they are being dragged towards the tail [37], [38], [39].

Scientists are still divided on this question while the evidence available is not yet decisive. Many papers discuss the mechanisms of plasma entry in relation to the CDPS (for example, [35], [38] [39] [40], [41], [42], [43], [44], [45]).

2. KH properties and elements of MHD theory

2.1. Basics of the KH instability.

The process was studied by Kelvin during the second part of the XIX century in parallel with (but independently of) Helmholtz. The instability of flows with velocity gradients carries the name of the two pioneers. Lord Kelvin is the famous Scottish physicist associated with the second law of thermodynamics, the mathematical physics of electricity and magnetism, and the first transoceanic telegraphic cable. He was also active in the study of the conservation of circulation in fluids, the instability of strata moving with different velocities, and the formation of sea waves (Kelvin, 1871). Helmholtz, the eminent German physicist who made important contributions to acoustics, thermodynamics, magnetism, and physical physiology, also studied the laws of vorticity in fluid mechanics. He investigated the instability of layers in relative motion, with applications to the case of clouds (Helmholtz, 1868) (The references to the original papers can be found in Chandrasekhar [46]).

A simple idea of the instability mechanism is the case of wind blowing over water with the growth of sea waves. The positive feedback is due to the Bernoulli's effect in subsonic flows: $p + \frac{1}{2}\rho u^2 = const.$; this is sketched in figure 1. The slowing down at the wave bottom becomes a place of higher pressure, while the increased speed at the wave top is a site of lower pressure than average.

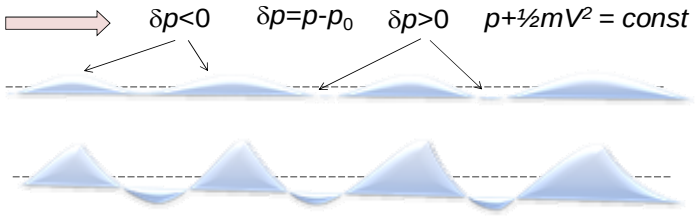

Figure 1. Wind-sea interaction. The wave growth arises from the positive feedback due to Bernouilli's effect for incompressible flows. In a wave hollow the speed slows down, and the pressure is larger than in the unperturbed state. By contrast, at a wave crest the speed increases, and the pressure is smaller than the equilibrium state.

The KH excitation can be examined from different points of view. In fluid dynamics considerable insight is gained from the study of the vorticity mechanism [46]. The energy flow approach is also illuminating, specially in plasmas because it can be extended to branches of the plasma wave spectrum other than the low frequency MHD oscillations, which are our main concern here. The presence of free energy in a velocity gradient flow can also be a source of growth for high frequency plasma waves. (for example, [47])

The energy method is described in figure 2. It represents a perturbed interface of counter-streaming flows, eventually observed from a moving frame, so that the velocity of the upper layer is parallel and opposite to that of the bottom. The physical quantities on either side of the interface are denoted by sub-indices 1, 2. The motion is along $\pm x$, and the equilibrium surface is the plane y=0. When perturbed by a wave, a sector one wavelength along x and unit length in z, that extends along y on one side, say y>0, has a smaller energy content than in the absence of undulation.

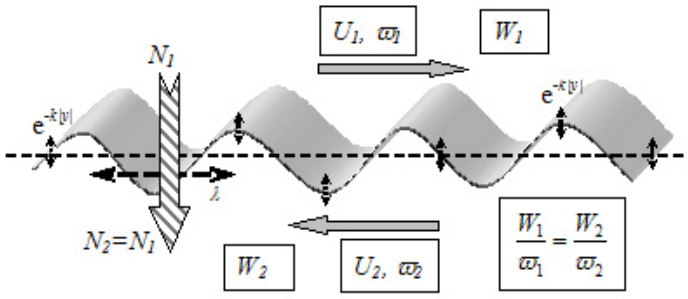

Figure 2. Energetics of the KH instability. Interface between two opposite moving layers with speeds U_1, U_2. The perturbation with wavenumber $k=2\pi/\lambda$ is localized near the interface, and decreases as exp(-$k|y|$) on both sides; ϖ_1, ϖ_2: Doppler shift frequencies, W_1, W_2, perturbation energy densities. Energy is transferred from one side to the other (zebra arrow) coupling negative with positive energy densities. The amplitude grows with no external energy sources. The process conserves the number of energy quanta, N_1, N_2 (see text).

Conversely, the twin sector that extends on the opposite side, y<0, has more energy than in equilibrium, and by the same amount. Accordingly, we can say that the energy of the perturbed state on the y>0 side is negative, while that of the other side y<0 is positive. The instability couples positive with negative energies across the surface. Energy flows from one side to the other, and the amplitude of the perturbation grows on both sides of the interface, with no need of external agents.

It can be shown that the ratio of Doppler-shifted frequencies on either sides, $\varpi_1/\varpi_2=(\omega-kV_1)/(\omega-kV_2)$ is negative in the unstable situation, and is equal to the ratio of the respective energy densities, W_1/W_2. This can be interpreted as the conservation of the number of energy quanta $N_1=W_1/\hbar\varpi_1=W_2/\hbar\varpi_2 = N_2$, in this process (for example, [48]).

Compressibility allows a coupling of KH perturbations with acoustic waves. This reduces the efficiency of the KH mechanism. To begin with, compressive KH modes have a penetration distance (normal to the interface) much larger than $\lambda/2\pi$, the range of influence of incompressible perturbations. When the magnetoacoustic coupling becomes significant, the same amount of energy is spread in a wider plasma volume, and the growth rate of the mode is reduced. Eventually, at sufficiently large supersonic speeds, the energy is radiated away from the surface by magnetoacoustic waves, and the mode cannot grow any further.

Figure 3 illustrates the effect: on the left, below a critical velocity V, a coupling of negative and positive perturbations leads to the instability; on the right, at a higher (supersonic) speed, the emission of a pair of acoustic waves (with positive and negative energy densities) takes place. The argument explains qualitatively the stabilizing effect of compressibility. The energy flux does not feed the growth of the surface perturbation, but goes away with the waves instead (e.g. [47], [49]).

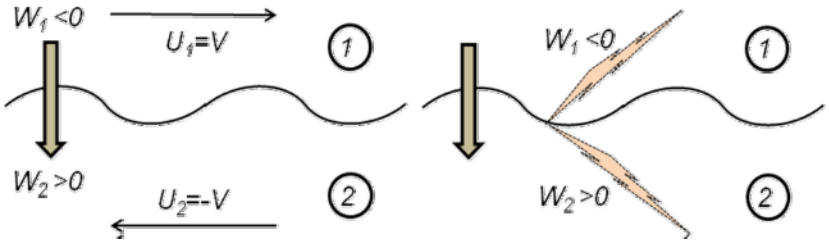

Figure 3. Schematic to illustrate the stabilizing effect of compressibility. Left panel: the energy flux feeds the growth of the interface perturbation for V less than a critical value. Right panel: at a larger speed the energy flux is radiated away by a pair of positive-negative energy acoustic waves.

Precise conditions for the KH instability in compressible MHD require an elaborate description. ([50], [51]). Briefly put, the BL is likely to be unstable when the magnetic shear angle through the transition is small, and/or when the Alfvénic Mach number is large, $M_A = \Delta U/V_A >>1$ (ΔU: velocity jump through the layer; V_A: Alfvén speed); we return to compressible KH in subsection 2.4.

2.2. MHD stability theory

In a region of flow with velocity shear the KH instability is driven by the projection of the velocity on the $\boldsymbol{k}$ vector, the wave-number of a perturbation mode. It is opposed by tensions associated with the magnetic field projection on the same $\boldsymbol{k}$-mode. The velocity and magnetic field components in the $\boldsymbol{k}$ direction are denoted with V_k, B_k, respectively,

$$V_k = \mathbf{V}\cdot\hat{\mathbf{h}}, \quad B_k = \mathbf{B}\cdot\hat{\mathbf{h}} \tag{1}$$

where $\hat{\boldsymbol{h}} = \boldsymbol{k}/|\boldsymbol{k}|$ is the unit vector along $\boldsymbol{k}$. The physical quantities on either side of the velocity gradient region are indicated with sub-indices 1, 2. In a MP context 1 is for the magnetosheath, and 2 for the magnetosphere.

In the simplest model the interface has no thickness, and the stability is computed in the incompressible MHD approximation. It is a planar tangential discontinuity (TD) with a difference of parallel velocities across it. Incompressible theory predicts stability of any given $\boldsymbol{k}$-mode when the following (necessary and sufficient) condition is satisfied,

$$\left\langle \left(V_k - \langle V_k \rangle\right)^2 \right\rangle \leq \left\langle V_{Ak}^2 \right\rangle, \tag{2}$$

(Gratton et al, 2004 [52]). The bracket < > indicates a weighted average of any physical quantity, *f*, defined as

$$\langle f \rangle = \left(\rho_1 f_1 + \rho_2 f_2\right)/\left(\rho_1 + \rho_2\right) \tag{3}$$

where ρ is the mass density. In condition (2) $V_{Ak}^2 = B_k^2/4\pi\rho$ is the square of the Alfvén speed computed with the magnetic field projection B_k, which embodies the effect of magnetic tensions. When the average of the square of the projected Alfvén speed is larger than the mean square of the projected velocity deviations of the average value, the mode is stable.

Stability condition (2) can be set in a more widely known [46], [53] equivalent form:

$$\rho_R \left(\Delta \mathbf{V} \cdot \hat{\mathbf{h}}\right)^2 \leq \left[\left(\mathbf{B}_1 \cdot \hat{\mathbf{h}}\right)^2 + \left(\mathbf{B}_2 \cdot \hat{\mathbf{h}}\right)^2 \right] \Big/ 4\pi \tag{4}$$

where ρ_R, defined by $1/\rho_R=(1/\rho_1 + 1/\rho_2)$, is a kind of "reduced" mass density, and $\Delta \boldsymbol{V} \equiv \boldsymbol{V}_1 - \boldsymbol{V}_2$ is the velocity difference across the surface. The TD model, also called as "thin" model in Farrugia et al., (1998) [54] is fully stable when the stability condition holds for all the directions of $\boldsymbol{k}$. The thin model stability does not depend on the wavelength.

Interestingly, condition (2) can be extended to a "thick" BL model [53], with a stratified planar geometry where the physical quantities are spread over (*x*, *z*) planes, and are represented by continuous functions of the coordinate *y* normal to the strata. The functions connect the physical values on both sides of a velocity gradient interface with finite width *D*. The form of the stability condition (2) for a thick model remains unchanged if the weighted average (3) is replaced by a new average with a weight $\mu_k(y)$:

$$\langle f \rangle_k = \int_{-\infty}^{+\infty} f(y)\mu_k(y)dy, \tag{5}$$

where the integration is over the whole range $-\infty<y<+\infty$ that extends across the BL model [52]. However, now the weight function $\mu_k(y)$ is mode-dependent. Here $\zeta_k = \zeta_k(y)$ is the $\boldsymbol{k}$-mode amplitude, and it is the solution of a boundary value problem for the stability equation of the thick model, equation 6. Stability of thick models depends not only on the direction of $\boldsymbol{k}$ but also on the wavelength.

The equation of the amplitude ζ (we now omit the sub-index for simplicity) in the incompressible approximation, is [53]

$$\frac{d}{dY}\left[H \frac{d\zeta}{dY} \right] - k^2 H \zeta = 0, \tag{6}$$

where

$$H(y) = \rho\left[\left(c - V_\kappa(y)\right)^2 - V_{A\kappa}{}^2(y)\right], \tag{7}$$

and *c* is the phase velocity of the modes, defined at equation (11), subsection 2.3 (where the compressible treatment is given). The term $\rho(y)V_{Ak}^2(y)$ represents the magnetic tension $B_k^2/4\pi$. In fact, the roots of $H = 0$ are transverse Alfvén waves that propagate with respect to the plasma flow

$$c - V_\kappa = \pm V_{A\kappa}(y), \tag{8}$$

The function $V_{Ak}^2(y)$ is a stabilizing agent, and cannot be switched off except when the magnetic field is unidirectional. A case in which modes with $B_k = 0$ for all *y* are possible (called *flute modes* in the literature). However, in general, the direction of the magnetic field is different on either side of the

interface, i.e., a rotation of the magnetic field direction occurs. Magnetic shear prevents the existence of flute modes, and is always a stabilizing factor.

Condition (2) takes the same form for both thin and thick models, although with a different averaging procedure, equations (3) and (5) respectively. It is, therefore, possible for a TD with given quantities on both sides of the interface to satisfy the stability condition, while a companion thick model connecting the same values with continuous functions may predict the presence of unstable modes.

This may seem odd since, as we approach the TD limit by decreasing the width of a thick model, the velocity gradient increases and it looks like the interface should become prone to the instability. When the thin model is unstable, the associated continuous model is certainly unstable, albeit with a reduced growth rate. But the converse is not true. A continuous model can be unstable at moderate wavelengths, comparable with the interface width, but long wavelengths may be stable. In the latter case the TD approximation is found to be stable [53].

The reason for the different behavior resides in a degree of flexibility allowed to ζ, the solutions of equation (6), which may assume shapes that reduce the contribution to the averages of condition (2) of y-ranges with large magnetic tensions, and enhance instead the effect of y-intervals with a dominant velocity gradient. This is in contrast to the rigidity of density as averaging weight. Of course, the increased freedom associated with ζ is possible only in continuous models, and is absent in the thin approximation case.

2.3. Stability equation and characteristic value problem.

In ideal (non resistive) compressible MHD the amplitude of the Fourier modes of KH perturbations is governed by the second order differential equation,

$$\frac{d}{dy}\left[H\left(1-\frac{1}{M}\right)\frac{d\zeta}{dy}\right]-k^2H\zeta=0, \tag{9}$$

(derived by Gratton et al., 1988 [55]). The modes are of the form

$$\Xi=\zeta(y)\exp(-i\omega t+ik_x x+ik_z z), \tag{10}$$

where Ξ is the y component of the Lagrangian displacement of a plasma element from the equilibrium position, and ζ is the corresponding amplitude. The wave-vector of the mode is represented by $\boldsymbol{k}=(k_x,0,k_z)$; the absolute value $k=|\boldsymbol{k}|$ and the angle φ between $\boldsymbol{k}$ and $\boldsymbol{V}$, also define the wave-vector properties.The (complex) angular frequency of the modes is denoted by $\omega=\omega_r+i\gamma$. The real part ω_r is the frequency of the perturbation, and the imaginary part γ is the temporal growth rate.

A complex phase velocity $c\equiv\omega/k$ is defined so that the coefficient $M(y)$ of the differential equation for ζ can be written as follows

$$M(y)=1-\frac{\left(V_A{}^2+c_s{}^2\right)}{(c-V_\kappa)^2}+\frac{V_{A\kappa}{}^2c_s{}^2}{(c-V_\kappa)^4}, \tag{11}$$

while the function $H(y)$ is the same as defined in subsection 2.2, equation (7). In equation (11) $V_A=B/\sqrt{4\pi\rho}$ is the Alfvén speed, c_s is the speed of sound, V_k, B_k are projections already defined (equation (1)), $V_{Ak}=B_k/\sqrt{4\pi\rho}$ is the projected Alfvén speed (subsection 2.1), and all these quantities are functions of y. We use hyperbolic functions with a scale length d, for example $V_x=\frac{1}{2}U_1[1+\tanh(y/d)]$ for the velocity field (where U_1 is the magnetosheath velocity). The x-axis is chosen along the flow direction. Similar expressions connect the other scalar and vector fields across the BL. A detailed description of the BL models for MP stability studies is given in Gnavi et al., 2009 [56].

The stability analysis belongs to the temporal class, in which the (real) wave-number $\boldsymbol{k}$ is given (a Fourier component of the initial perturbation), and the response of the system determines the unknown

(complex) value of c. This is a characteristic value problem for equation (9) subject to the boundary conditions, $\zeta \to 0$ for $y \to \pm\infty$.

When $c_s \to \infty$, the coefficient $M \to \infty$, and equation (9) reduces to the incompressible approximation, equation (6). In this case the asymptotic behavior of ζ is fixed on both sides as $\exp(\pm ky)$, $y \to \pm\infty$. If the transition layer is very thin with respect to the wavelength, that is when $kd << 1$ (where $d = \frac{1}{4}D$ is the scale length of the hyperbolic functions, associated to the width D of the BL), a dispersion relation can be obtained integrating equation (6) across the discontinuity (assumed to be at $y=0$). Using decreasing exponentials solutions on either sides, we obtain the dispersion relation of the thin model

$$H_1 + H_2 = 0\,, \tag{12}$$

where H_1 and H_2 are the values taken by H on each side. Equation (12) then readily leads to the stability conditions (2)-(4).

2.4. Influence of compressibility

Condition (2) for thin or thick models is restricted to the incompressible approximation. Compressibility can stabilizes KH modes as noted in subsection 2.1. When ρ is constant across the TD, and $\Delta\boldsymbol{V}\cdot\boldsymbol{B} = 0$ (or in the absence of a magnetic field; $\Delta\boldsymbol{V}$ is the velocity difference across the interface), the stability condition with $\boldsymbol{k}$ parallel to the flow is $M_s > 2$ (derived by Landau, 1944 [57]) where M_s is the sonic Mach number defined by $M_s = |\Delta\boldsymbol{V}|/c_S$.

But this result is valid only for $\boldsymbol{k}$ aligned with the flow. When $\Delta V_k = \Delta\boldsymbol{V}\cdot\hat{\boldsymbol{h}}$ is less than the speed of sound, and this occurs when $\boldsymbol{k}$ turns away from $\Delta\boldsymbol{V}$, the corresponding modes are still unstable, although with reduced growth rates because the instability is not driven by the full impact of the velocity difference. In addition, when a magnetic field is also present as in MHD, the instability that remains in modes with $\boldsymbol{k}$ at an angle with $\Delta\boldsymbol{V}$ may still be suppressed. This happens when a rotation of $\boldsymbol{k}$ away from $\Delta\boldsymbol{V}$ brings $\boldsymbol{k}$ closer to the $\boldsymbol{B}$ direction, so that adverse magnetic tensions ($B_k^2/4\pi$) are switched-on, or augmented. Moreover, the critical value $M_s > 2$ for parallel $\boldsymbol{k}$ stability holds only for equal densities across the interface. But the critical condition is very sensitive to changes of the density ratio ρ_2/ρ_1, as we shall find in section 4.

For large $|y|$ ($|y|/d >> 1$) all quantities attain their constant values on both sides of the boundary layer, and indicating with M_1, M_2 the constant values of the coefficient M on each side, the solutions of equation (9) tend asymptotically to

$$\zeta \to A_1 \exp\left(-ky\sqrt{\frac{M_1}{M_1 - 1}}\right), \qquad y > 0$$

$$\zeta \to A_2 \exp\left(+ky\sqrt{\frac{M_2}{M_2 - 1}}\right), \qquad y < 0\,, \tag{13}$$

The KH modes are perturbations localized at the interface, and tend to zero on both sides of the MP, that is, $\zeta \to 0$ when $y \to \pm\infty$. Therefore, the branch of the square root must be defined as

$$\kappa \equiv \Re\left(k\sqrt{\frac{M_a}{M_a - 1}}\right) \geq 0\,, \qquad a = 1,2\,. \tag{14}$$

In the case of unstable modes, $\Im(c) > 0$ the M_a are complex valued, and the square root has also an imaginary part. Therefore, when $|y|/d >> 1$ while the mode amplitude tends to zero, it also oscillates spatially along y. Ordinarily $\kappa \sim O(k)$, so that the penetration depth of the perturbation on either side is

usually of order $1/k=\lambda/2\pi$. Except when $M_a\approx 0$, when the influence of the perturbation extends far on both sides of the transition.

The roots of $M=0$, the coefficient that distinguish compressible (9) from incompressible (6) behavior, are the phase velocities of MHD fast and slow modes (with respect to the projected plasma velocity),

$$(c-V_\kappa)^2=\frac{1}{2}\left(V_A{}^2+c_s{}^2\right)\pm\frac{1}{2}\sqrt{\left(V_A{}^2+c_s{}^2\right)^2-4V_{A\kappa}{}^2c_s{}^2} \tag{15}$$

Thus, when M takes small values, $M<<1$, a coupling of the KH mode with magnetoacoustic waves is expected The perturbation extends over a larger volume than in the incompressible case, and eventually energy is lost by emission of acoustic waves (subsection 2.1).

The extension from the incompressible thin case to the (more complicated) compressible thin model was studied by González and Gratton, 1994 [50]. The compressible dispersion relation is given by

$$H_1\sqrt{\frac{M_1}{M_1-1}}+H_2\sqrt{\frac{M_2}{M_2-1}}=0 \tag{16}$$

where the square roots must have positive real parts, condition (14). Due to this constraint the dispersion relation is non algebraic. When we express this as a polynomial, spurious roots are introduced. Numerical work is required, and for this reason the compressible thin model does not lead to a simple exact formula, as the incompressible thin case. An instability condition like (2) or (4) is not available. The role of magnetic tensions in counteracting the velocity difference drive is subject to the intervention of magnetoacoustic effects.

The stability conditions for supersonic magnetospheric flanks are intricate because of density and temperature asymmetries between magnetosheath and magnetosphere. Theory indicates that the stabilizing action of compressibility is a strong function of the density ratio $r_d=\rho_2/\rho_1$ across the transition. Moreover, the KH stability condition of a BL modeled by continuous profiles for $\boldsymbol{B}$, $\boldsymbol{V}$ and ρ can be very different from the stability predicted by the TD approximation in common use [53]. In addition, the efficiency of the stabilizing effects depends on the local values of M_s and M_A, and the angle between $\boldsymbol{B}$ and $\boldsymbol{V}$. A stability treatment tailored to each specific configuration under study is necessary. These points rise in the study of the special event examined in sections 4 and 5.

3. Topics of magnetopause research

3.1. Instability bands on the dayside MP

A basic tenet of the front-side model of Farrugia et al. [22], [54], for a northward IMF with small $|B_y|/B_z|$, is that KH activity resides in two bands whose width increases with decreasing B_y (field components are in the GSM system; see for example [8]). The inputs for the stability study are based on a theoretical MHD model of the dayside MP with a paraboloid shape that interacts with the solar wind. The external flow is matched with a compressed geomagnetic dipole field inside the diurnal magnetosphere.

Views of the velocity field with black arrows, and local magnetic shear angle with a color scale over the dayside MP surface, are shown in figure 4 for two IMF clock angles (angle θ of the IMF with the geomagnetic north; positive when $B_y>0$), 20° left panel, and 5° right panel. In the figure the surface is a frontside view (from $X>0$) of the MP model with a solar wind stagnation point flow at the center. The coordinates X, Y, Z are in the GSM system with center at the Earth; X points to the Sun, Z to the geomagnetic north, and Y completes the orthogonal triad, with $Y>0$ pointing to dusk.

An important feature of this model is that the MHD stagnation point flow is compelled to move normal to the local magnetic field, so that the KH instability is excited mainly with modes $\boldsymbol{k}\perp\boldsymbol{B}$. The KH-active strips are bands of low magnetic shear (i.e.,with nearly-parallel magnetic fields on either

sides of the MP). In the northern hemisphere they extend eastward (and vice-versa in the southern). As θ decreases, the bands widen until, for due northward IMF, all the low latitude MP away from noon is KH-active, and the MP near noon is KH active to higher latitudes (compare the two figures). Clearly, north-south and dawn-dusk asymmetries in dayside KH activity are implied by this model. Their existence poses a challenge to any interpretation of mass transfer by mechanisms other than KH. Moreover, the unstable bands are sources of KH waves that are convected toward the flanks, and while moving tailward they may develop, under favorable conditions, into full size vortices.

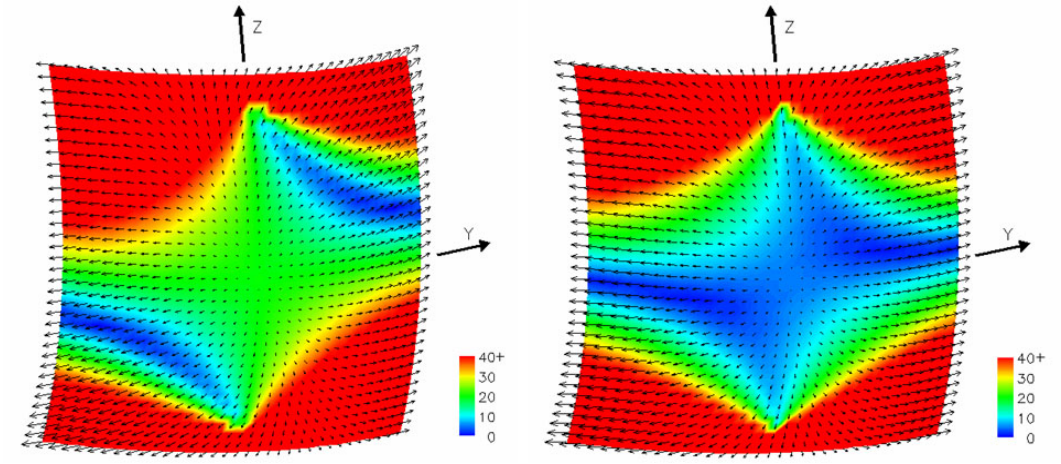

Figure 4. An illustration of the dayside instability bands according to Farrugia et al. [54]. The surface is a front side view (from X>0) of a MP model, with the solar wind stagnation point flow at the center; X, Y, Z are GSM coordinates. Small black arrows represent the velocity field, and the color scale of different areas indicates the local magnetic shear angle. The left panel is for the IMF clock angle of θ=20°, while the right panel is for θ=5°.

Indirect experimental support for the unstable bands theory was found via the agreement of changes of the Pc5 power spectra with variations of the clock angle [58].

KH perturbations of the MP can couple with resonances in the front side magnetospheric cavity. Surface perturbations are transmitted into the magnetosphere, and resonate at magnetic shells, known as L-shells, where resonance conditions for transverse Alfvén waves are satisfied [59]. The wave that couples the surface waves with resonating magnetic lines is a magnetosonic mode, since it must transport energy across the field. The excitation of the resonant magnetic lines was confirmed, both by spacecraft observation and by ground magnetometers, for ULF (*ultra low frequency*) magnetospheric waves. They correspond to Pc5 geomagnetic perturbations (2.5 to 10 minutes periods).

The CME which passed Earth on April 11, 1997 afforded an excellent opportunity of studying KH activity at the dayside magnetopause as a function of the clock angle θ of the IMF. Figure 5 shows data taken by Wind on April 11, 1997, the z component of the field (GSM system) and θ from 8 to 20 UT. The magnetic field is strongly north in the interval 10 to 14 UT, which is favorable for KH excitation.

From, approximately, 10 to 12 UT the average clock angle is 18° and after that, in the following lapse 12-14 UT, the average clock angle decreases to 6°. We can appreciate in figure 4 the important increase of low magnetic shear areas, from the first to the second period.

The Pc5 power spectral density of the high latitude chain of ground magnetometers, IMAGE, computed for the two mentioned time intervals, is represented in figure 6. The plots clearly display an increase of power, and a shift to lower frequencies, when the second time period is compared with the first. The dayside band theory gives an interpretation of these facts: for θ = 18° only short wavelengths that fit into small band areas can be unstable, while for θ = 6° with larger areas available longer

wavelenghts for unstable modes are possible. The KH frequency is proportional to the inverse of the wavelength, so that more room for the instability at lower frequencies is available.

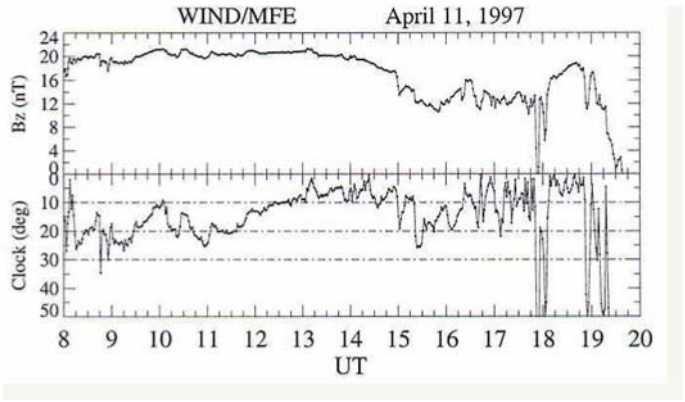

Figure 5. Data from Wind on April 11, 1997: the *z* component of the magnetic field (GSM system) and the clock angle of the IMF, θ, from 8 to 20 UT (see text).

In our research of the KH excitation on the dayside MP the presence of a plasma depletion layer (PDL) was included in the MP model [53], [54], [60]. This is a layer with a strong magnetic field (due to convection pile-up) and low density that appears in the subsolar región of the magnetopause, usually under northward IMF conditions. The *PDL* should be considered in studies of dayside MP stability as the outer boundary condition. The *PDL* also affects the critical M_A value predicted by Fuselier et al., 2000 [45] that regulates the competition between KH and tearing mechanisms (on which we return in subsection 3.3), as well as the density ratio across the MP, and it is therefore a significant element to bear in mind in stability studies for this region.

In modeling the MP transition the use of continuous field profiles is necessary. As we have shown [52], [53], the oft-quoted criterion for KH instability of the MP, which assumes it to be a TD, can be misleading when predicting stability. For a subsonic dayside physical regime, we found that there are unstable modes with $\lambda \sim 2.5\ D$ (where *D* is the thickness of the transition) with significant growth rates, which are stable under the same boundary values according to the TD approximation. Hence, the stability analysis with a TD model can miss the KH excitation altogether.

With Cluster and Themis crossings of the dayside MP under steady northward IMF conditions, and on both sides of noon, further progress can be made on this matter. More advanced global models could be a valuable help. Another point is to find the ionospheric signatures of the KH-active bands at the MP. This requires the mapping of the KH unstable bands of the dayside MP to the ionosphere.

3.2. Stability of dayside pristine MPs: the effect of transient periods of compression and expansion.
The difference in ground response to Kelvin-Helmholtz instability of the dayside MP for two different IMF θ (the clock angle) orientations described in subsection 3.1 is reduced by the presence of a low latitude boundary layer (LLBL) [54]. The dependence of KH activity on θ should be most clearly observed in pristine magnetopauses, i.e., those that occur without an adjoining magnetospheric boundary layer. Pristine MP are about a 10 % of a statistical study of data crossings of the frontside magnetopause [61]. They show very sharp density gradients, with a thickness δ for density transition, much smaller than the thickness Δ of the current layer, $\delta << \Delta$. Ratios 1:5 and less has been observed.

We comment on calculations that take into account two length scales, Δ and δ, in the equilibrium fields. Together with a velocity gradient, the effect of a transient acceleration *g* of the MP is included, which is the driver of the Rayleigh-Taylor (RT) instability (Gratton et al., 1996 [62]). The acceleration of the dayside surface happens during lapses of fast expansion, or compression of the magnetosphere,

following changes of solar wind properties. At small wavelengths, the results with $\delta/\Delta<<1$ differ substantially from those for $\delta/\Delta = 1$, and suggest new tests of correlations between spacecraft observations, and ground magnetometer data.

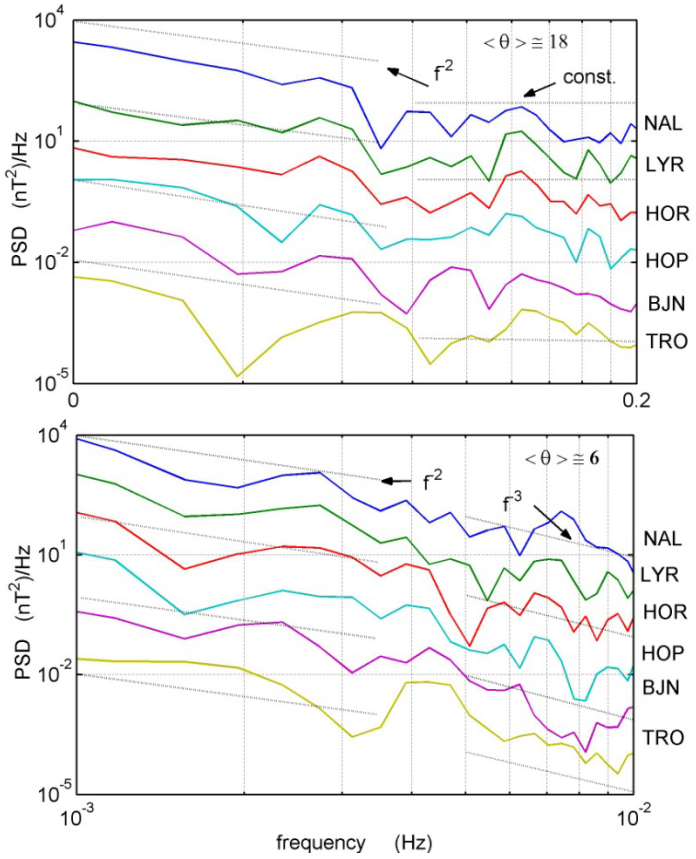

Figure 6. Power spectral density in the Pc5 range of a chain of high latitude ground magnetometers for two time intervals, from 10 to 12 UT, upper panel, and from 12 to14 UT, lower panel. The plots show an increase of power, and a shift to lower frequencies, from the second to the first time period.

MHD perturbations of a simple MP model without low latitude boundary layer, display the basic trends effortlessly. This is a model where changes of the physical quantities take place over two very different length scales as in figure 7. The schematic show a velocity gradient transition with a small scale density drop, represented by a discontinuity. The profile for B_κ is similar to V_κ.

The Kelvin - Helmholtz instability operates over relatively long stretches of time, in sites where the action of the velocity gradient prevails over stabilizing magnetic forces. Conversely, the Rayleigh-Taylor instability is a transient process which appears during episodes of magnetopause acceleration, as a result of rapid changes of solar wind dynamic pressure. Since the magnetosheath expands or contracts together with the magnetopause, in a neighborhood of this boundary nothing changes locally, except for the acceleration of the site in toto.

For ordinary fluids with stratified density, G. I. Taylor showed that regarding stability the effect of a global acceleration was mathematically equivalent to the effect of gravitation studied earlier by Lord Rayleigh (references cited in [46]). Physically, this is an example of Einstein's equivalence principle.

In the simplified theory the density profile is represented by a discontinuity. WKB approximations, with $\lambda<<\Delta$, are used in the velocity gradient regions at either side of the discontinuity, and matched across the density jump. It is easy to derive the dispersion relation,

$$\omega = kV_k + \frac{1}{2}\left(\frac{\rho_1-\rho_2}{\rho_1+\rho_2}\right)DV_k \pm \sqrt{\frac{1}{4}\left(\frac{\rho_1-\rho_2}{\rho_1+\rho_2}\right)^2 (DV_k)^2 + \left[\frac{2k^2 B_k{}^2}{4\pi(\rho_1+\rho_2)} - gk\frac{\rho_1-\rho_2}{\rho_1+\rho_2}\right]} \quad (17)$$

where the growth rate is given by $\gamma = Im(\omega) > 0$. Here V_k and B_k stand for the projections of $\boldsymbol{u}$ and $\boldsymbol{B}$, on the $\boldsymbol{k}$ vector of a Fourier mode. DV_k denotes the V_k gradient across the magnetopause. The quantities B_k, V_k, DV_k, assumed to be continuous, are computed at the density jump; density appears with both side values, ρ_1 for the magnetosheath, and ρ_2 for the magnetosphere $\rho_1 > \rho_2$; $g>0$ corresponds to a sunward acceleration (MP expansion).

The dispersion relation equation (17) is computed in the incompressible limit for subsonic speeds (but compressibility corrections to the main instability branch can ordinarily be neglected on the dayside MP). The whole derivation is discussed in Gratton et al., 2003 [63].

If $\gamma = 0$ the modes are stable, and when $g=0$ the formula shows the typical absence of the KH instability for small λ. Interestingly, when $g>0$ the Rayleigh-Taylor effect is stabilized, or at least reduced, by the presence of the velocity gradient DV_k, even for flute modes where $B_k = 0$. On the other hand, in the phase of acceleration towards the Earth, $g < 0$, the modes with $\lambda << \Delta$ are stable, flute or not. Equation (17) can be contrasted with the long wavelength, $\lambda >> \Delta$, subsonic dispersion relation

$$\omega = k\frac{\rho_1 V_{\kappa 1} + \rho_2 V_{\kappa 2}}{\rho_1 + \rho_2} \pm \sqrt{\left[\frac{B_{\kappa 1}^2 + B_{\kappa 2}^2}{4\pi(\rho_1 + \rho_2)} - \frac{\rho_1 \rho_2}{(\rho_1 + \rho_2)^2}(V_{\kappa 1} - V_{\kappa 2})^2\right]k^2 - gk\frac{\rho_1 - \rho_2}{\rho_1 + \rho_2}} \quad (18)$$

which follows directly from the incompressible stability equation of the thin model (including g),

$$H_1 + H_2 + kg(\rho_1 - \rho_2) = 0 \quad (19)$$

The roles of the velocity gradient in the former case, and the velocity difference in the latter, are inverted. Therefore, the instability due to the joint factors has a transition from large $\lambda >> \Delta$, where the KH and RT (with $g>0$) effects add together to amplify the perturbation, to small λ where the velocity gradient works in opposition to the RT mechanism, and may even produce stability in a definite range of small $\lambda \approx \Delta$ (although for very small $\lambda << \Delta$ the RT becomes dominant again).

From the scaling law of the equations it follows that the influence of the RT action as an activating mechanism of the KH instability is more intense during a slow solar wind period than in a fast one. Within lapses of fast solar wind streams the importance of transient accelerations on KH excitation is expected to be reduced [63].

3.3. KH and tearing modes at the MP

That velocity shears can hinder the onset of tearing modes [64] was noted in plasma physics with the discovery in the 1990s of the H-mode Tokamak operation. It was found that a differential rotational flow in the device could suppress reconnection of magnetic surfaces and improve plasma confinement. A number of theoretical studies have been published since, having to do not only with Tokamak physics but also with more generic shear flows of plasmas dealing with KH and tearing effects ([65] and references therein). For space plasmas early influential studies were those of La Belle-Hamer et al., 1995 [41], and Chen et al., 1997 [44].

About the same time this question became a hot topic in space physics because of the great interest aroused by encounters with cold, dense plasma sheets under northward IMF conditions. As mentioned in section 1.3, CDPS compositional studies showed to be of magnetosheath origin [66] (Fuselier et al., 1999). Reconnection poleward of the cusps is a possible candidate. But under northward IMF conditions the KH instability can be operative as well. Many subsequent papers on the issue have struggled with these entry mechanisms ([39], [41], [43], [44], [45], [66], [68], [69], [70], [71]). In the absence of crucial evidence, the question is whether other processes such as diffusive entry [42] and the KH instability [28], [31], [35], may contribute to the formation of the CDPS.

A basic conclusion of the theoretical work for flows with constant density, is that the presence of velocity shear indeed interferes with the tearing process when the Alfven Mach number, $M_A > 1$. The tearing modes are stable in super-Alfvenic flows, where the KH instability predominates. An example of this assertion is illustrated by figure 8 which shows the competition between KH and tearing modes

in a plasma model with magnetic shear and a velocity gradient flow (Bender, Ph.D. Thesis, 1997 [72], and Bender et al. 1998 [73]). The theory is MHD equations with resistivity and viscosity included.

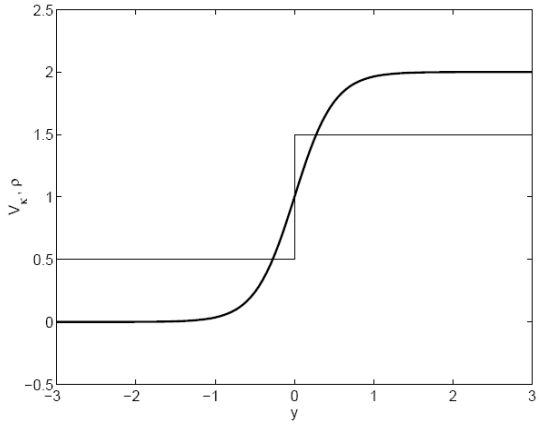

Figure 7. A velocity gradient interface with a small scale density drop, represented by a discontinuity. Field profiles for a WKB analysis: velocity V_κ and density ρ versus y ($y>0$ points toward the MS). The trend for B_κ is similar to V_κ.

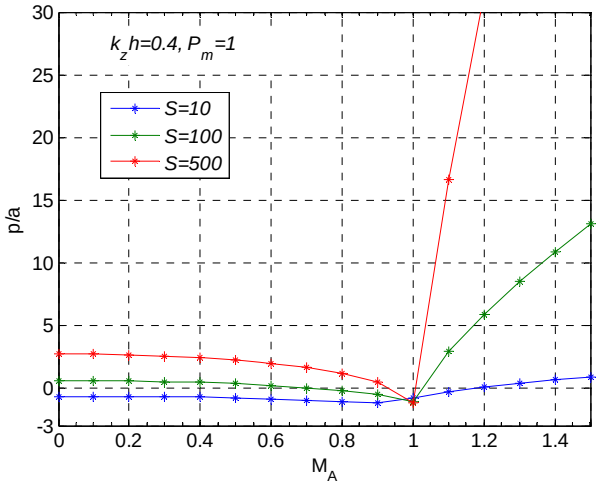

Figure 8. Competition between KH and tearing modes. The plot shows a normalized growth rate p/a versus M_A, for a fixed normalized wavenumber $k_z h$=0.4 and magnetic Prandtl number P_m=1, for three values of the Lundquist number S (see text). For M_A <1 there is tearing instability and no KH excitation, vice versa when M_A >1 tearing is quenched and there is only KH instability.

Here the perturbation modes have the functional dependence $A(y)exp(pt+ik_z z)$, where $A(y)$ stands for the modes amplitude. Figure 8 shows the normalized growth rate p/a versus M_A, for a given normalized wavenumber $k_z h$=0.4 and a fixed magnetic Prandtl number P_m=1.

Across a boundary layer model, stratified in y and layered on planes (x, z) which is at the same time a current sheath and vorticity layer, the main flow $V_z=V_z(y)$ is counter-streaming, and the magnetic field $B_z=B_z(y)$ changes sign at y=0. The resistive and viscous structure is maintained in steady state against diffusive effects by an additional stagnation point flow $V_x=ax$, $V_y=-ay$, where a is the strain rate of this secondary flow ($e_{xx}=\partial V_x/\partial x=a=-\partial V_y/\partial y=-e_{yy}$). The boundary layer scale length along y is represented by h, and is used also to normalize k_z. The magnetic Prandtl number $P_m=\nu/\nu_m$ is the ratio of viscous and resistive kinematic diffusivities.

The colored traces in figure 8 are for several values of the Lundquist number, $S=V_A/(a/\nu_m)^{1/2}$. When M_A <1, only the tearing modes are excited, with a growth rate that diminishes as the resistive effect decreases. By contrast, when M_A >1 the tearing modes are stabilized by the flow, and only KH modes that overcome magnetic tensions are amplified. It was noted, however, that the precise value of M_A at which tearing is inhibited depends on the density ratio across the layer.

In his thesis work Bender [72] found also that the critical M_A value that suppress the tearing effect depends in a significant way on the magnetic Prandtl $P_m=\nu/\nu_m$. [73]. The classic theory of plasma transport predicts a strong dependence of P_m with temperature [74]. However, in a non-collisional plasma as the interplanetary medium it is expected that P_m is determined mainly by anomalous effects related to the micro-fluctuation level of wave fields. On waves in the space environment of the Earth see, for example, [58], [75], [76], and the literature quoted therein.

On the other hand a small-scale tearing process may enhance the efficiency of diffusive transport inside large KH eddies formed in the BL. This is a possible cooperation of tearing with KH (in the

non-linear stage) in the sense that rolled-up vortices may stretch and bring into contact oppositely-directed field lines which then reconnect. In the MP context this effect was emphasized by e.g. Otto and Fairfield (2000) [28], and others. The concept was known in MHD much earlier, by way of 2D simulations of vortices that wound weak magnetic fields into coil shapes [77] (Weiss 1966). The magnetic field lines yield passively to the strength of the flow. It was found that the whirling motion intensify the dissipation rate of the magnetic field, via a sequence of tearing and reconnection events.

To conclude, despite important research progress the knowledge of the actual influence of velocity shear on tearing, and vice versa, in the magnetopause context is still incomplete. Some elements of the problem have not yet received proper attention, but can make substantial contributions in assessing the merits of the mass entry mechanisms.

3.4. Gaps of KH amplification at the flanks.

The MP flanks have been repeatedly visited by spacecraft under different magnetosheath conditions, and at different latitudes and downtail distances. The many configurations encountered may now be catalogued as a function of these quantities, and their stability examined systematically. The stability of flows with velocity shear is strongly affected by compressibility when the flow becomes supersonic, as it does on the flanks.

The main question is to find when is a flank region is KH-unstable. What are the onset conditions for supersonic flows? How does the broadening of the flank BL, produced by the KH instability, depend on (i) the local orientation of $\boldsymbol{B}$ and $\boldsymbol{V}$, (ii) the physical conditions at the boundary, and (iii) its distance from the subsolar point?

KH amplification may have gaps, i.e., regions of local stability, on the flanks (Gnavi et al. 2009 [56]). Consider the solar wind with a northward IMF in the magnetosheath at a near Earth flank position, where the flow is again moving at supersonic speeds. We investigate the theoretical conditions required for the Kelvin-Helmholtz modes of the magnetopause to be stable. The stability is studied with an equilibrium model of the low latitude boundary layer (LLBL) described by hyperbolic tangent profiles for the main scalar, and vector fields, ρ, T, $\boldsymbol{V}$, $\boldsymbol{B}$, of a MHD treatment. The BL thickness $D=4d$ (as in subsection 2.2) is a free parameter of the calculation that can be adjusted at the end, according to observation inputs or judicious conjectures.

KH stability (or negligible growth rate) is possible when the sonic Mach number $M_s=U_1/c_s$ (U_1, c_s, flow speed and sound speed of the adjacent MS, respectively) is larger than but close to one, $M_s\sim1.3$, while the Alfvénic Mach number $M_A=U_1/V_A$ (where V_A is the MS Alfvén velocity) remains a bit smaller than one, $M_A\leq1.2$. Local stability of the LLBL is found when, combined with the quoted Mach number values, there is a significant magnetic shear angle between the IMF and the geomagnetic field. Solar wind with physical conditions favorable to the stability of near Earth flanks, are cold and not too dense plasmas, with rather strong magnetic fields. Such that M_A is rather smaller, while M is somewhat larger, than the average values of ordinary solar winds. These conditions are often realized during the passage of the tail of CMEs by Earth.

We computed several stability cases of the equatorial flanks. The boundary layer parameters are inputs from spacecraft crossings, complemented by judicious extrapolations of the physical conditions expected upstream, and downstream of the orbits. We reach the conclusion that when the above-mentioned features materialize a gap between KH amplifying regions at the near equatorial flank can be expected. The KH instability of the unstable strips of the front side [54] convected to the flanks may traverse a neutral amplification region before reaching the MP tail. The distant flanks are again unstable because of the enfeeblement of the geomagnetic field toward the magnetosphere tail.

On the other hand, when large-scale vortices are observed in the flank BL the question is how far upstream they are generated. Under the conditions discussed it may happen that the origin is not distant a few amplification lengths upstream, but a far away area in the unstable bands of the dayside.

An example is shown in figure 9. In this case the geomagnetic field is somewhat stronger than the outer field. The flow is supersonic $M = U_1/c_s=1.4$, and slightly super Alfvénic $M_A= U_1/V_A=1.2$, while the magnetic shear angle across the LLBL is 45 °. After optimization over k, and the angle φ of $\boldsymbol{k}$ with

the flow, the (normalized) maximum growth rate (for φ=15°) is already very small. An e-folding time of growth, assuming $D = 6000$ km and $U_1 = 300$ km/s, can be estimated as τ = ½ hour. Moving a degree upstream, where M =1.2, M_A =1, which corresponds to a U_1 decrease by a 20 % (keeping the other fields at the same values) no growth is found, the LLBL is locally stable. A stability gap, between the dayside unstable bands and the unstable distant MP tail, is present.

Note that for very long wavelengths (the range near kd=0) the growth rate becomes zero at a small kd value. This means that a thin model of the LLBL (a tangential discontinuity, *TD*) fails to perceive the existence of an instability for M=1.2, M_A=1.4. What we called a "*pitfall*" of the *TD* model [53] occurs also in supersonic flows. It is worth keeping this in mind at downstream sites, where γ becomes significant while a TD approximation may still forecast a stable MP. Finally, further downstream near the tail, the instability chances improve because M_A, M, increase together with U_1 while the magnetic tensions in the BL become weaker with the decline of the geomagnetic field.

The parameters of the event of January 11, 1997 studied in [67] provide another example. This is again a possible scenario with a non-amplifying gap in the near flank. The magnetosheath values are: U_1=300km/s, B_1=30 nT, θ_1=100°, n_1=10 p/cm^3, T_1=0.130 keV. On the magnetosphere side: B_2=20 nT, θ_2=30°, n_2=1 p/cm^3, T_2=1.9 keV. The Mach numbers in this case are M_s=1.90, M_A=1.67. The maximum growth rate occurs for kd=0.65, λ≈4.8 R_E, assuming a width ≈1 R_E, and the e-folding time is τ_e≈3.5 min. The ***k-V*** angle for the maximum growth rate is φ=- 4.33°, and modes with a deviation of Δφ ≈±15° from the optimal ***k*** orientation are stable [56].

Figure 10 represent the normalized growth rate versus changes of M_s. The ratios of the physical quantities, and the angles of the fields are maintained constant, except the two Mach numbers that vary together keeping a constant ratio M_s/M_A=1.14.

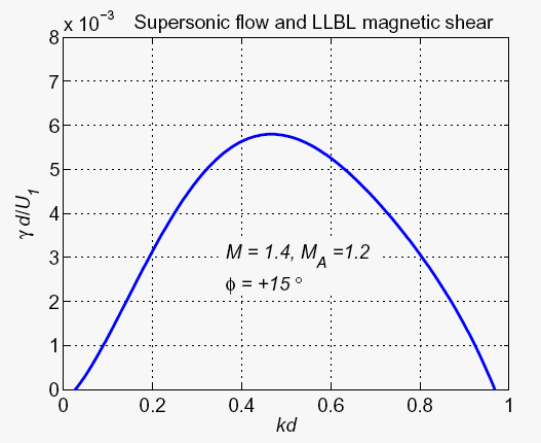

Figure 9. Normalized growth rate $g=\gamma d/U_1$ as function of non-dimensional wave number, kd. The model is specified with hyperbolic functions. The magnetic shear angle across the LLBL is 45 °, and the ratio B_2/B_1 is a bit larger than 1.The ***k*** direction is for the maximum growth rate (ϕ=15° with the x-axis). The Mach numbers are $M_s = U_1/c_s$ =1.4, and $M_A = U_1/V_A$ =1.2. Note that for small kd values (≤0.03) the modes are stable (see text). The instability is weak and not far upstream, where U_1 is 20% smaller, there is no growth

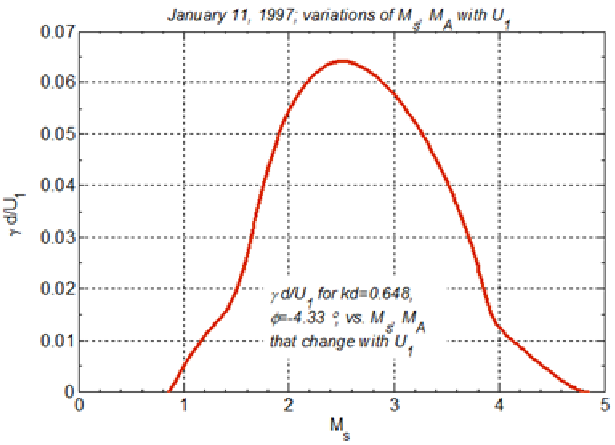

Figure 10. Scenario for the January 11, 1997, event [67]. Another case that shows possible stable gaps in the flanks. Normalized growth rate versus changes of M_s. All the other quantities are maintained constant while both Mach numbers vary jointly (see text).

This can be a consequence of changes of the magnetosheath velocity U_1. The change may be associated with variations of the solar wind speed, or with a choice of different positions along the flank. The growth rate has a maximum for $M_s \approx 2.5$, but the instability declines both for $M_s < 2.5$, and $M_s > 2.5$ (upstream or downstream, respectively, if we interpret the variations as changes of site). For $M_s > 2.5$ the stability is due to the influence of compressibility. For $M_s < 2.5$ the effect of magnetic tensions prevails. The results emphasize the importance of using data from actual spacecraft crossings to initiate stability studies with realistic features. It also bears on the size and width of the dayside KH-active bands, mentioned in subsection 3.1, which continuously feed KH perturbations that travel tailward with the flow. Examples of the interplay of these elements can be found in [51], [56], [67], [78], [79], [80]. Several years of data from flank crossings (including MP skimming orbits) mainly from Cluster and Geotail, and recently Themis are now available to address these issues. Cluster and Themis can provide simultaneous multi-point observations at key entry locations, which may allow boundary conditions to be set from measurements made near the locale whose stability is being examined. A noteworthy attempt was done by Paschmann et al. (2005) [81], who characterized the MP and BL in the dawnside near-tail, based on 24 crossings in a single Cluster skimming orbit. A systematic survey of flank crossings, classifying them by their characteristics and input parameters for BL models, along the lines mentioned, especially during CMEs passage, is desirable so that stability criteria for each representative class can be properly investigated.

4. The event of October 24, 2001 and stability analysis

4.1. ACE and Wind observations

We report a research on vortices observed in the BL on October 24, 2001, and the stability of that layer. The magnetosheath field was approximately parallel to the flow direction (albeit pointing sunward), as studied in detail by Farrugia et al., 2010 [82]. The interest of this event resides in the peculiar field orientation, different from the northward IMF of most investigations on the KH instability, and the recognition that it can provide knowledge concerning also the much more frequent case of Parker's spiral field.

A plasma flow with a parallel magnetic field is not a favorable configuration for the Kelvin-Helmholtz instability, because magnetic tensions in full action operate to stabilize the configuration. In particular, this happens at the stagnation point region of the dayside MS. Near the subsolar point the solar wind slows down to $M_A<1$, and is dominated by magnetic tensions. From there, the MS plasma speeds up again along the flanks, where M_A increases and eventually exceeds unity. Hence the KH mechanism could start t but the issue is not straightforward, because the motion at the flanks is supersonic, and compressibility cooperates with magnetic tensions to favor stability (as noted in section 2). The instability may occur perhaps too far tailward to explain the origin of the vortices observed in the BL during a Wind´s crossing. This is the problem we adress here.

The magnetosheath is shaped by the solar wind characteristics, and the bow-shock transition. The event we consider occurs during the last phase of the passage of a multiple ICME group by Earth. A description of the interplanetary physics during the days 21-25 October, 2001 is given in [82], [83]. The distinctive trait of the late hours of October 24, 2001, is a quiet and steady plasma, with an almost radial speed and magnetic field.

Figure 11 displays the solar wind data registered from 18 to 21 UT by ACE during the event. This period comprises the interval of interest, from 19 to 20:30 UT, when vortical perturbations were observed in a Wind crossing of the BL.

We focus our attention on this time interval. ACE's time scale has been adjusted by the time delay for the interplanetary plasma to reach the region of Wind's orbit. The first row of Figure 11 presents: the magnetic field intensity B (black), almost constant at 6 nT, and the three components in GSM coordinates B_x, (red) B_y (green) and B_z (blue). In the interval 19 to 20:30 UT B_x is also quite steady, less than B only by a small extent, and positive. The other components are small, and the angle of the field with respect to the flow oscillates slightly between 164°-159° (shear angle, seventh row). The

field is approximately antiparallel to the flow, which is almost radial (antisunward) with a moderate speed, $V \approx 370$ km/s, indicated in the fourth row. The second and third rows are for particle density, $N_p \approx 4$ p/cm^3, and temperature $T \approx 4 \times 10^3$ °K, respectively. The plasma is very cold and field-dominated, with a plasma beta $\beta \approx 0.02$ (fifth row). These physical conditions are frequent in CMEs. The dynamic pressure is shown in the sixth row, $P_d \approx 1$ nP.

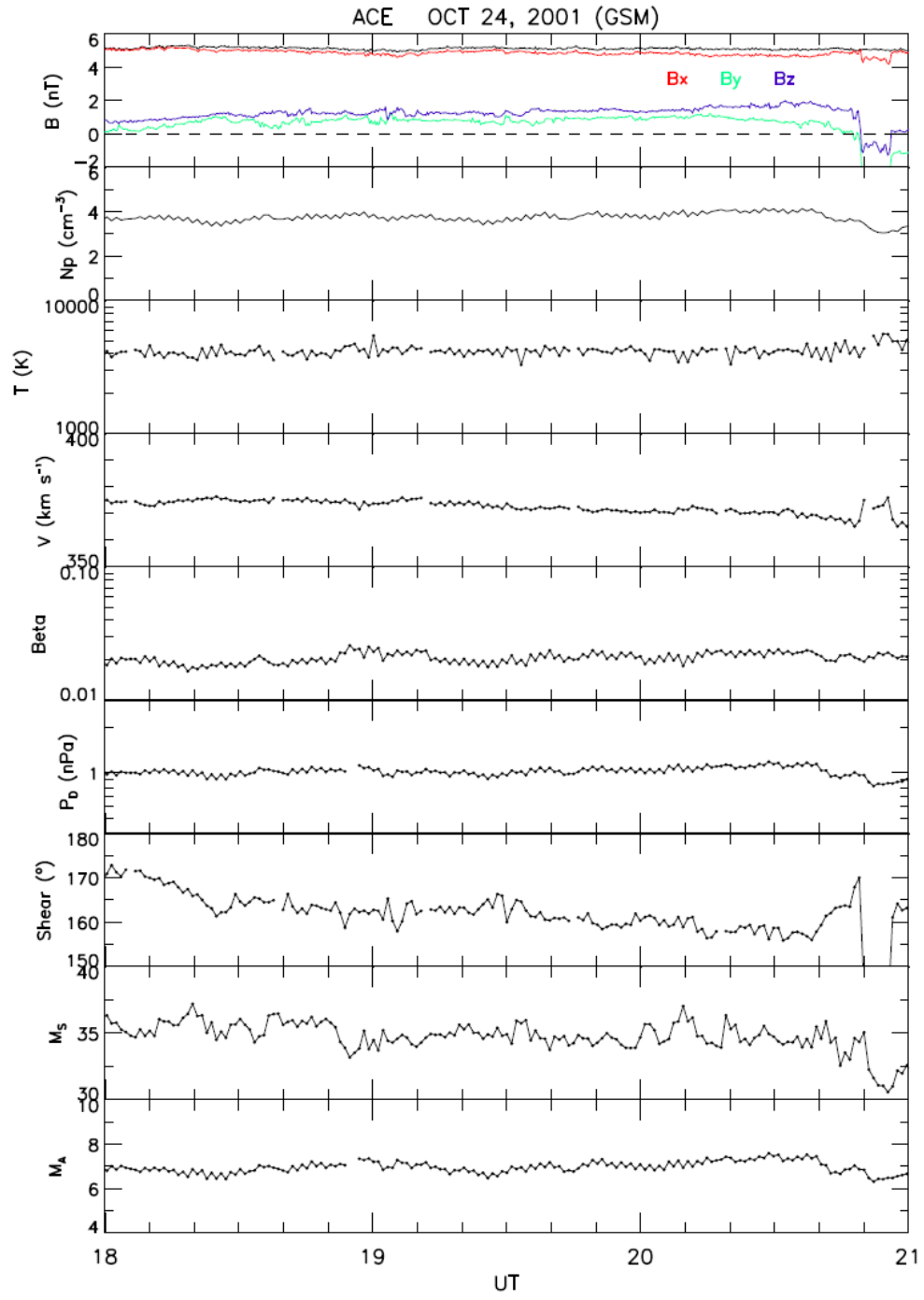

Figure 11. ACE interplanetary data from 18 – 21 UT, October 24, 2001, covering the time interval 19 – 20:30 of Wind traversal of the boundary layer. ACE time is shifted by the delay of the solar wind to reach Wind's position (for details see text).

To conclude: the quiet solar wind recorded by ACE has a moderate speed, but given the prevailing magnetic field strength, density, and very low plasma temperature, it flows steadily at an unusually high sonic Mach number, $M_s \sim 34$, and a rather large Alfvenic Mach number, $M_A \sim 6.5$ (last two rows). The Mach numbers M_s, M_A of the solar wind are connected to the corresponding magnetosheath Mach numbers by a MHD theory of collinear flows (subsection 4.3).

We come now to Wind's observations. The orbit (see a plot in [82]) is easily described as follows. At 19 UT Wind enters the BL from the magnetospheric side at (-14.1, -22.8, 6.1) R_E (GSM coordinates) and at (-13.7, -25.0, 5.3) R_E, at 20:30 UT, exits into the magnetosheath. Wind was moving mainly dawnward at a downtail distance X ~ -14 Re, an orbit's segment roughly normal to the local boundary layer. It is an orbit ideal to observe the dynamics during a complete traverse, and to evaluate the width of the BL.

Crossing the equatorial dawnside plasma sheet/LLBL, Wind observed the quasi-periodic field and flow disturbances shown in figure 12. From top to bottom, the proton density, p/cm^3 (with a logarithmic scale), the plasma speed (absolute value) km/s, the proton temperature °K (logarithmic scale), and the magnetic field (absolute value) nT. Then follow the velocity components (km/s), and the magnetic field components (nT), respectively, in GSM coordinates X,Y, Z.

The pulsed character of N and T, with the quasi-periodic, alternating hot-tenuous and cold-dense plasma, is already hinting at a motion of organized structures over the spacecraft. A series of 15 perturbations of this type are recorded. The impression of a passage of billows with two classes of organized plasma is accentuated by the well correlated, and periodical, spiky pattern of B_x, B_y, and also (with somewhat less definition) of V_x, V_y. Note that while the magnetic record is uninterrupted, the plasma measurements show a few gaps due to instrument problems. The following step is to find a plausible explanation of the BL observations

4.2. Stability of collinear magnetic field and flow

The MP from dayside onward is subject to the impact of waves and fluctuations coming from the magnetosheath. The waves transfer momentum across MP, from the solar wind into the boundary layer. The result is equivalent to a viscous drag of the adjacent magnetospheric plasma (the so called "pseudo-viscosity"). Plasma close to the boundary is dragged along by the solar wind. Therefore, a velocity shear flow is established inside the boundary layer.

On the equatorial dayside up to the terminator, the flow near the inner edge of the boundary layer is practically normal to the geomagnetic field, and it is subsonic (because of the reduced speed in the LLBL, and the higher temperature of the magnetosphere). The physical conditions at the inner edge side of the BL are very different from those of the outer limit, contiguous to the field-aligned flow. On the magnetospheric side of the BL, although the velocity is reduced with respect to MS, the development of the KH is easier when we consider flute modes. By this we intend modes with $\boldsymbol{k}$ normal to the (geomagnetic) field, and therefore parallel to the flow. Thus, we expect that in the October 24, 2001 event the inner part of the boundary layer is the first to become unstable.

The vector and scalar fields chosen for the discussion of the KH instability on the front side of the magnetosphere, where the BL perturbations observed further down-tail start, are of necessity based on ACE observations supplemented by theory, in view of the absence of spacecrafts monitoring the dayside magnetosheath. In the unperturbed model the magnetic field $\boldsymbol{B}$ is assumed collinear with the flow $\boldsymbol{V}$, anti-parallel to it as revealed (approximately) by ACE's observations. As in section 2, the analysis uses a local x-axis set in the direction of $\boldsymbol{V}$ (so that only the V_x component is different from zero). The y-axis is normal to the MP pointing outward. Completing the triad, the z-axis is oriented in the same sense as the geomagnetic north (the x-axis direction is opposite to that of the GSM X coordinate). The magnetic field in the adjacent magnetosphere is assumed to be perpendicular to the flow direction, in the sense of the geomagnetic field. Thus, the magnetic shear angle of the model is 90° (clockwise, looking from $+y$).

Presumably, this angle is not exactly 90° and varies with the distance to the subsolar point. We expect that at equatorial latitudes the deviations from 90° are not substantial. Anyway, this choice is

not particularly biased in favor of the instability, because we intend to switch-off, or at least reduce, the magnetic tensions on the magnetospheric side of the BL by considering ***k***-modes normal to the local geomagnetic field. This ***k*** orientation maximizes the V_k contribution to the instability, but exposes the mode to the full stabilizing capacity of the magnetosheath field (B_k component).

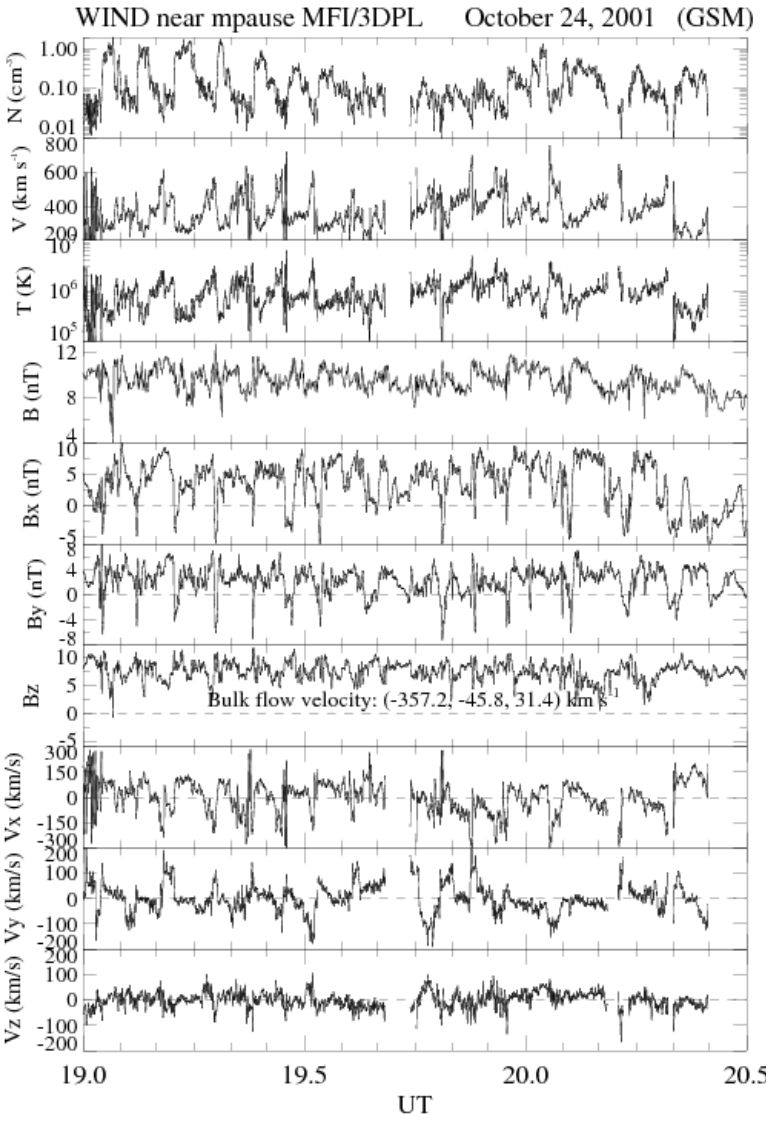

Figure 12. General view of Wind's records during the BL crossing of October 24, 2001, from 19.0 to 20.5 UT, decimal hours. From top to bottom, proton density p/cm^3 (logarithmic scale), plasma speed (absolute value) km/s, proton temperature °K (logarithmic scale), magnetic field intensity, nT. Then follow the velocity components (km/s), and the magnetic field components (nT), respectively, in GSM coordinates.

At the near-Earth MP we assume a typical particle density ratio n_2/n_1=0.1, and magnetic field intensity ratios B_2/B_1=1.4-1, with a stronger field in the magnetosphere. The highest ratio is an upper bound enforced by the need to preserve pressure balance across the MP. All quantities are normalized with their MS values, and both Mach numbers, M_s, M_A are computed with parameters of that region. Figure 13 illustrates an example of basic functions used in the stability calculation. In the first panel are represented n, V_x, B=|***B***|, with blue, green, and red lines respectively, and in the third panel, B^2, χ

with blue and green lines, respectively. Here χ denotes the magnetic shear angle (the angle of $\boldsymbol{B}$ with the x-axis, since field and flow are collinear). Together with n and B^2, χ determines the temperature change across the BL via a pressure balance equation. The second (central) panel of figure 13 shows the projections V_k, B_k. They are important functions that decide the outcome of the stability study, as we have seen in section 2.

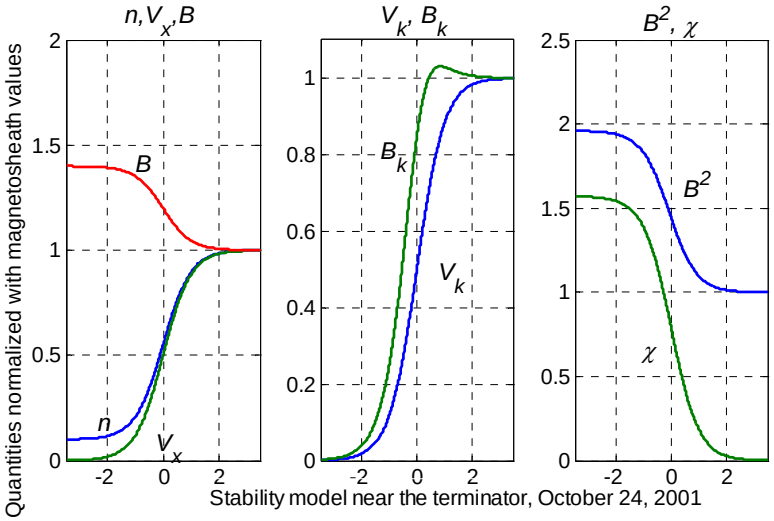

Figure 13. An example of the set of functions that appear in the equations of the compressible MHD stability analysis for a BL model. Right panel: B, n, and V_x as functions of y/d, red, blue and green lines, respectively. Center panel: B_k, V_k vs. y/d, green and blue lines, respectively. Left panel, B^2, χ, vs. y/d, blue and green lines, respectively. See text for the meaning and role of these functions.

4.3. Stability near the terminator.

For near-Earth scenarios the physical quantities for the MS, and the Mach numbers, are based on the Spreiter and Rizzi 1974 [84] theory, which gives an approximate representation of the transition from solar wind before the bow-shock to the magnetosheath, for collinear MHD flows. In the absence of direct experimental information we use the Spreiter-Rizzi solution with solar wind data from ACE as inputs. Close to Earth at the MP terminator, the theory predicts approximately M_s=7.7, M_A =4.9.

We begin with an interesting result of the thin approximation shown in figure 14, computed from equation (16) with these Mach numbers, and other quantities as in subsection 4.2. Keeping other parameters fixed the density ratio is changed. The instability appears only in a restricted range of density ratios, ρ_2/ρ_1 ~ 0.03 - 0.43. The equal density case is seen to be stable in agreement with Landau's theory. The growth rate γ has a maximum near ρ_2/ρ_1 ~ 0.1; γ is normalized with kU_1 since a thin model has no width. For a rule of thumb comparison with a thick model at the maximum growth rate, one may take roughly k~1/D (D: width of the BL).

The fact that a supersonic (and super Alfvénic) TD model may be stable both for small, and large ρ_2/ρ_1 values, is in line with results of the case of Wind's data input. As discussed at the end of this section, with a density ratio ~ 0.01 (but somewhat different parameters) the region of Wind's crossing is also found stable in the long wavelength limit.

The analysis for an hyperbolic functions model at the terminator is computed with the field and flow properties of subsection 4.2 and the previous Mach numbers. We assume a magnetic field ratio $r_B \equiv B_2/B_1$=1, which is sufficiently representative (γ is not very sensitive to r_B changes in the range 1-1.4). The magnetic tensions, whose influence decrease with the square of M_A, are reduced in their importance with respect to subsolar regions with small velocities near the stagnation point.

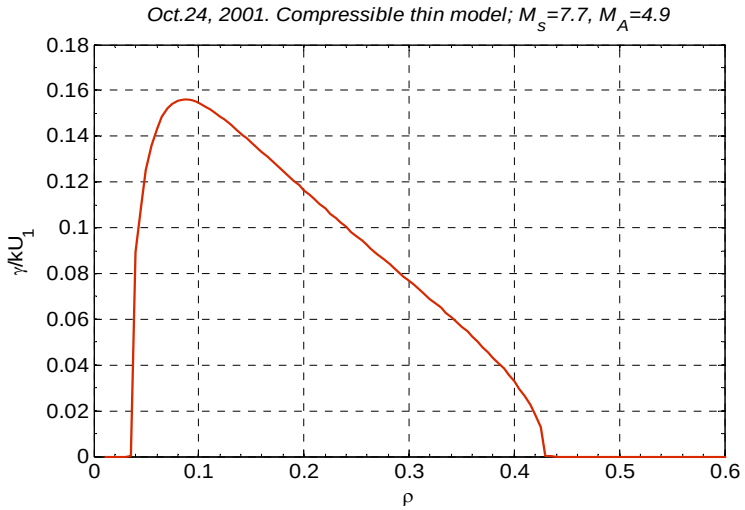

Figure 14. Growth rate γ (normalized with kU_1) versus variations of density ratio $\rho=\rho_2/\rho_1$. Thin model results with inputs from Spreiter-Rizzi theory applied to the magnetosheath near the MP terminator.

The result is given in two plots. Figure 15(a) presents the (normalized) growth rate, $\gamma d/U_1$ as a function of kd (modeled with hyperbolic functions with scale length d), while figure 15(b) shows $\Im(c)=\gamma/kU_1$, the imaginary part of the characteristic value c. An interesting feature appears in this range of parameters. The imaginary part of the KH dispersion relation, $\Im$(c), is a linear function of kd in most of the interval (for $kd\geq 0.15$). The growth rate is therefore a quadratic function k. For kd= 0.245 the (normalized) growth rate attains a maximum, $\gamma d/U_1=0.0195$. From this value we may estimate the e-folding time $\tau=1/\gamma\sim 137$ s for sites near the terminator. We use $D=0.5R_E$, assuming that the BL has not been yet broadened by the instability, and U_1=300 km/s. Hence, in a boundary layer not yet expanded by KH vortices, the growth of the perturbation proceeds at a fair pace.

The kd value for maximum γ is smaller than that of the cases of subsection 3.4, and leads to $\lambda\sim 6.41D$ for the KH waves of fastest growth. Given the long spatial size of KH perturbations over the MP, where wavelengths about tenfold times R_E have been reported [23], it is opportune to note that a stretching effect acts on the wavelengths. This is due to the speed increment from the dayside to the flanks. The effect is already present in the linear phase of the instability. For instance, starting near the subsolar point with a $\boldsymbol{k}$ vector pointing east, the wave front is convected downtail faster than the slow moving rear of the perturbation [85]. This generates an effective increment of the wavelength over the large extensions of the magnetosphere flanks.

4.4. Stability at the position of Wind's orbit

In the following case the model is prepared with data recorded by Wind along the orbit across the BL. The scenario is built from average magnetospheric measurements, before but near the entrance to the LLBL, including some initial part of the passage through it. On the other hand, we use averages of data recorded later, when Wind is in the magnetosheath.

The LLBL is already perturbed by the passage of the vortical structures, formed at some place near Earth. It could be argued that a local stability test is insecure because one inputs quantities that are already modified by the instability. Obviously, the remark does not apply to stable MP regions. When the site is ostensibly perturbed, (a) one should use only asymptotic values on either side, and leave the width of the transition as a free parameter of the study, and (b) with averages of perturbed quantities across the BL as input, one can still estimate whether the background posses amplifying power. The latter point means that in the case of intermittence, the KH activity may resume spontaneously.

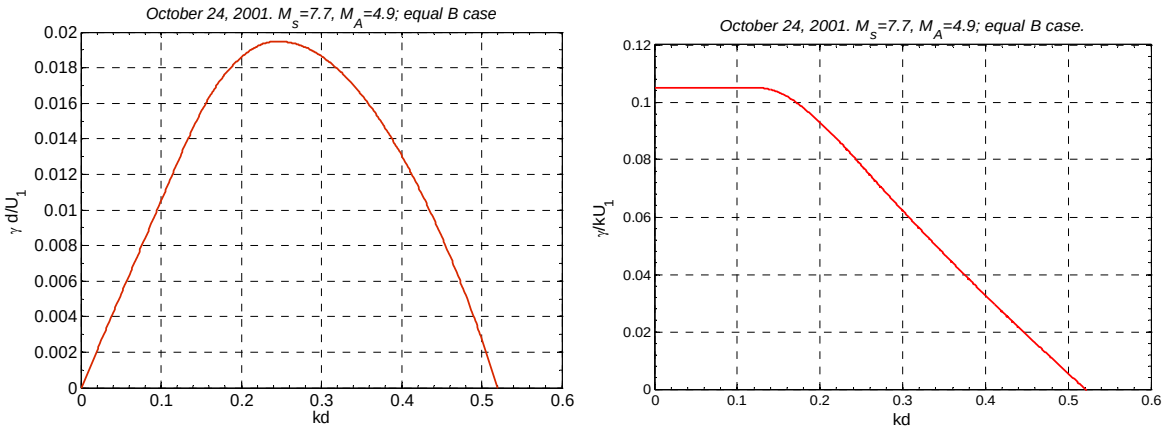

Figure 15. (a) (left) Normalized growth rate as a function of *kd* for the hyperbolic functions BL model at the terminator (see text). (b) (rigth) Imaginary part of the phase velocity *c* versus *kd*, for the same case of figure 15(a). $\Im(c)$ is a (decreasing) linear function of *k*, for *kd*>0.15.

The averages include long stretches of time on either sides of the LLBL, because the instability is found for long wavelenghts, of several R_E. At Wind's position, with a magnetosheath average velocity of 300 km/s, the Mach numbers are M_s=5.6 and M_A=6.8. The c_s that enters in the sonic Mach number is the plasma ion sound speed $c_s=(\Gamma k_B T_e/m_i)^{1/2}$, defined with the electron temperature and the ion mass. We assume $T_e=T_i$, (because T_e is not available in the data) and the specific heaths ratio is Γ=5/3. Unlike the terminator example, the magnetic shear is not 90° but rather 71° with respect to the sunward direction (derived from the magnetospheric side ***B*** average). Observations confirm that ***B*** is still approximately collinear with the magnetosheath flow. To sum up, the input parameters for the stability analysis are as follows. Magnetosheath: V_{1x}=300 km/s, n_1=5 p/cm³, $T_1=2.5\times10^5$ °K, B_1=4.5 nT, χ_1=0°, M_s =5.6 , M_A =6.8. Magnetosphere: V_{2x}=0 km/s, $n_2=5\times10^{-2}$ p/cm³, $T_2=2.0\times10^6$ °K, B_2=9.5 nT, χ_2=129° (the values comply approximately with pressure balance).

Note that the average magnetosheath speed adjacent to the BL is smaller than the ACE records ~370 km/s, and smaller than the bulk speed inside the BL (again close to 370 km/s) where vortical processes are going on. In the magnetosheath the gas presssure and the magnetic pressure are of the same order, but on the magnetosphere side the pressure is almost purely magnetic, the gas pressure being very small.

Figure 16 illustrates the results for this case. The plot at 16(a) shows the normalized growth rate $\gamma d/U_1$, as a function of *kd*. This is a case of stability at long wavelengths, i.e., *kd*<<1. For$\rho_2/\rho_1=10^{-2}$, the growth rate is zero when 0 <*kd*<0.07. It has a maximum $\gamma d/U_1$=0.033 at *kd*=0.43 and goes to zero at *kd*≈0.07 (long λ) and *kd*=0.84 (short λ). Figure 16(b) displays the behaviour of the imaginary part $\Im(c)$ as a function of *kd*.

Figure 17 presents the results of a thin model with the present local parameters. The growth rate (normalized "ad hoc" with *kd*~0.3) and $\Im(c)$ are plotted as functions of the change of both Mach numbers keeping fixed their ratio M_s/M_A =1.21 (for instance, as the consequence of changes of U_1). The thin model is stable for M_s =5.6, in agreement with the continuous model, and we note that the long wavelength approximation becomes unstable only when $M_s=1.21M_A\geq7.7$.

This analysis intends to show that a BL model, endowed with quantities represented by mean values of magnetospheric, and magnetosheath data, is unstable. The result is an indication that at Wind's orbit position, the boundary retains the property to augment fluctuations. If the passage of vortices is temporarily suspended, the background has the capability to rise perturbations, and to roll-over the layer again.

To conclude, the theory shows that the long series of large amplitude perturbations observed by Wind is compatible with a KH origin. The instability is possible in spite of the adverse configuration of field and flow. The outcome clears the way for the interpretation of data in terms of KH vortices.

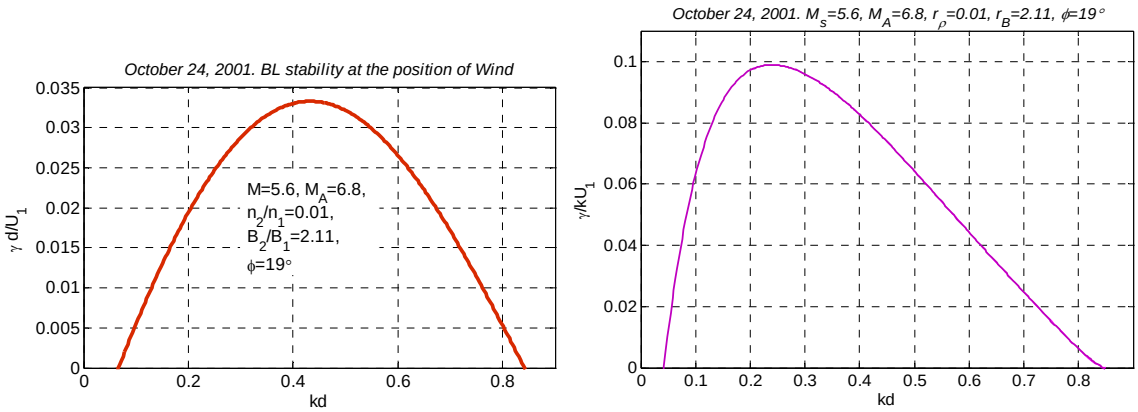

Figure 16. (a) (left) Normalized growth rate. (b) (right) Imaginary part of the phase velocity (normalized). Data inputs from Wind´s crossing.

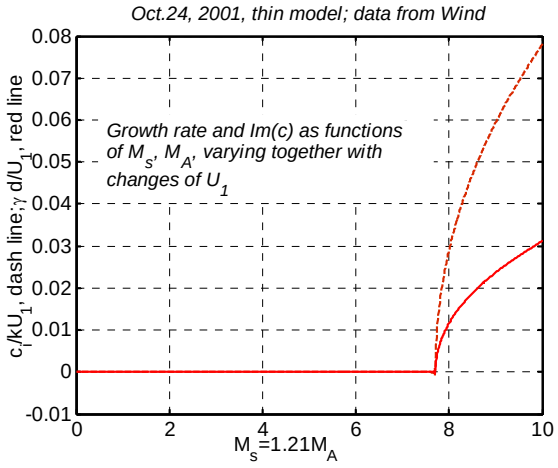

Figure 17. Thin model results with data from Wind. BL stability with Wind's input as a function of changes of Mach numbers (see text). The TD model becomes unstable only when M_s=1.21 $M_A \geq$7.7.

5. Experimental evidence of vortices

5.1. Data record details and interpretive key.

The data plotted in figure 18, with physical details of the third structure observed by Wind since the entrance in the BL, is representative of many other members of the series. The time interval (19.20 – 19.31 UT, approximately) includes a characteristic episode of cold-dense and hot-tenuous plasma alternation. The velocity components V_x, V_y, are averaged over the interval and the deviations dV_x=<V_x-<V_x>>, dV_y=<V_y-<V_y>> are plotted (km/s) with dashed blue, and dashed red lines respectively (the vertical scale is in km/s). The magnetic field components B_x, B_y are the solid green, and solid magenta lines, respectively (the magnetic field scale is enlarged 20 times, 20 units = 1 nT). In the same figure a dotted black line represents the number of particle density (scale enlarged 100 times, 100 units= 1 p/cm^3). The latter is added to visualize the phases of dense and tenuous plasma.

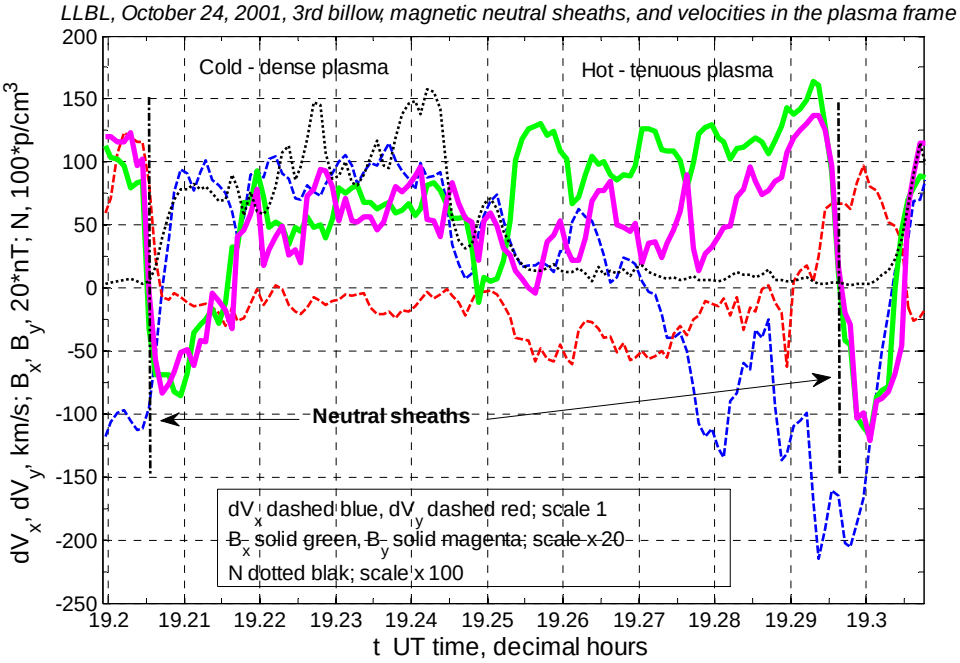

Figure 18. Details of the physical state of the third vortex observed by Wind. The presence of current layers is emphasized with black dashed lines. These are neutral sheaths that separate field components with opposite signs.

The dense plasma lags behind, in the average velocity frame it appears to move sunward. Conversely, the tenuous plasma moves in advance of the average, and proceeds fast tailward. The deviation dV_x attains important positive (+150 km/s), and negative (-200 km/s) values. Note that the average $<V_x> \approx$ -360 km/s is already moving faster than the adjacent magnetosheath flow average (-300 km/s), close to the solar wind speed before the bow-shock. The plasma structures are subject to an acceleration process operating in the BL.

The other important point of figure 18 is the presence of current sheaths, thin neutral layers across which the magnetic field components change sign (indicated by dashed vertical lines). The current sheaths appear in the transitions from hot-tenuous to cold-dense plasmas, they are absent in the reverse passage. The B_x-B_y components are fairly well correlated, B_x is mostly positive, in agreement with the collinear field of the magnetosheath, B_y generally points duskward (to the magnetosphere). Exceptions occur at hot-tenuous to cold-dense passages, where the spiky changes of magnetic sign take place. The current sheaths are signatures of a strain process of the collinear magnetic field lines, which are frozen-in the plasma and are being convected by the structures.

Figure 19 helps to visualize better the change of directions of the *x*-*y* magnetic and velocity components for the same third billow observed by Wind. We show arrow plots for the magnetic field B_x-B_y in the upper panel, and for the velocity deviations dV_x-dV_y ,in the lower part. The rotational pattern of the *x*-*y* velocity components at the transition from hot-tenuous to cold-dense plasma is apparent. It occurs at the positions where the *x*-*y* magnetic field components change sign, and the current sheaths are formed. The dashed lines in the bottom panel mark the separation of plasma in two classes by density and temperature.

5.2. Consequences of scatter plot analysis

Clearly, rolled-up vortices are a central concern in magnetopause physics. We have an MP crossing by a single spacecraft. What then, is it possible vortex detection by a single spacecraft? A peculiar

signature (Takagi et al., 2006 [86]) allows rolled-up vortices to still be identified. Their simulations show that the tailward speed of a fraction of low-density magnetospheric plasma exceeds that of the magnetosheath flow. This feature appears only after a vortex is rolled up. We apply this rule to the special field and flow configuration observed on October 24, 2001.

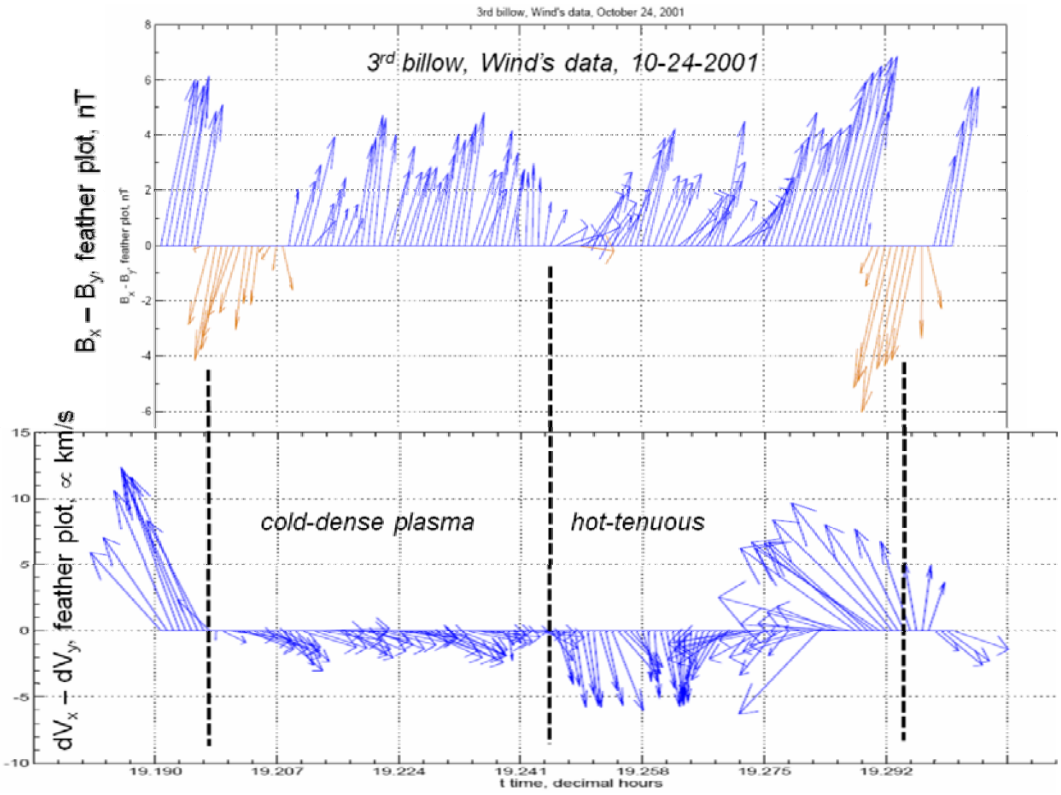

Figure 19. Arrow plots for the magnetic field B_x-B_y and the velocity dV_x-dV_y components, corresponding to the third vortex observed by Wind. The rotational pattern of the x-y velocity components at the transition from hot-tenuous and cold-dense plasma is apparent. It occurs at the same position where the x-y magnetic field components change sign, and the current sheaths are formed.

The vortex hypothesis accepted, qualitative pictures like figure 20 can be used as interpretive data tools. Figure 20 shows a vortex turn-over example, adapted from a MHD simulation. The cold-dense matter (in violet colors) of the upper layers (moving to the right) rolls back with a dense tongue, which embraces a hot-tenuous protuberance (in blue colors) that emerges from the bottom. The black dashed line indicates the (apparent) spacecraft motion relative to the vortex. The alternate cold-dense and hot-tenuous series makes sense immediately as the passage of a row of vortices that stir magnetosheath with magnetosphere plasmas. Another consequence is that the collinear field convected by the plasma motion tend to be coiled-up in the vortices.

Statistically more pregnant is the analysis of the whole set of LLBL data, represented in figure 21. We present a scatter-plot of dV_x (km/s) versus n p/cm^3 with a logarithmic scale (dV_x is the deviation of V_x from the mean value). To improve the visibility of the temperature trend, both the marker's size and the color are associated with T. The size is $\propto T$, large size for hot, and small size for cold matter. The color is $\propto \ln(T)$ (logarithmic scale is used because of the great difference of values), red for high, and blue for low temperatures.

Clearly, a significant fraction of the low-density, high-temperature plasma is flowing (tailward) at speeds well in excess of the bulk average of the BL, and much faster than the contiguous

magnetosheath speed. In agreement with the rule of [86] we have a sequence of rolled-up vortices passing by the spacecraft. We can also note that in the average frame, an important population of cold-dense plasma is moving sunward at considerable speeds. It is evident that a fraction of cold-dense magnetosheath plasma is turning back, and a majority of magnetospheric plasma is being accelerated toward the tail at high speeds. Even without the support of a simulation, the data alone give compelling evidence of a rotational motion superposed to a bulk translation.

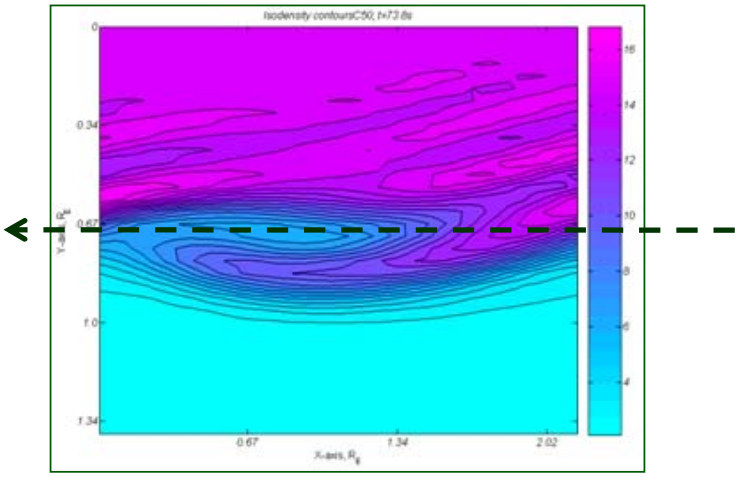

Figure 20. A vortex turn-over-over example (from a MHD simulation). Cold-dense matter (violet colors) from the upper layers rolls back with a dense tongue that embraces a hot-tenuous protuberance (blue colors) originated in the bottom layers. The black dashed line indicates the (apparent) spacecraft motion relative to the vortex. The cartoon helps as interpretive data tool.

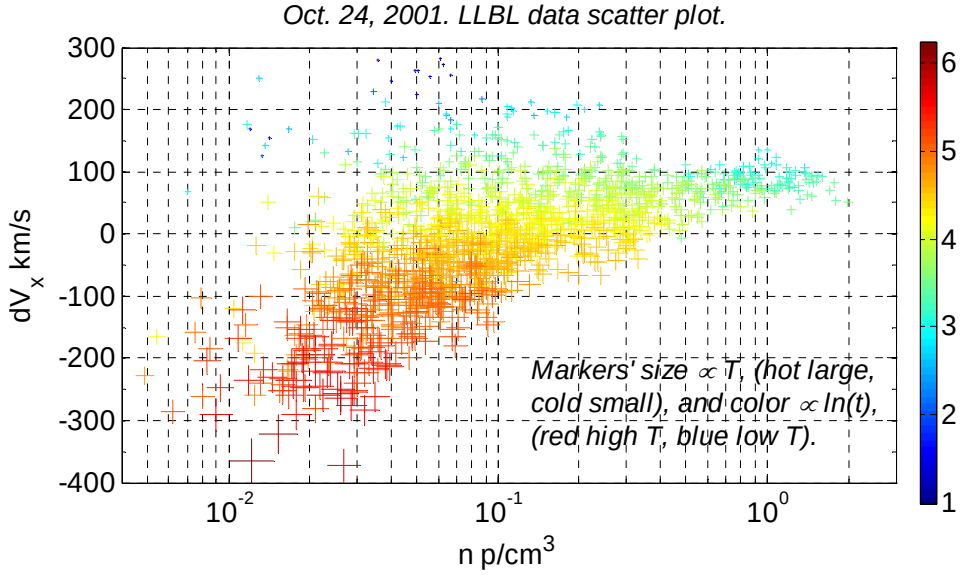

Figure 21. Scatter plot of dV_x km/s versus n p/cm3 for the whole LLBL data set. dV_x is the deviation of V_x from the mean value. Both, marker's size and color are associated with T, to improve the visibility of the temperature trend. The size is $\propto T$, large for hot, and small for cold matter. The color is $\propto \ln(T)$ (logarithmic scale because of the great difference of values), red for high, and blue for low T.

The statistics is complemented by the scatter-plot of figure 22. This is a correlation of dV_y versus dV_x also with the whole BL data set. To add information the marker´s size is proportional to the number of particle density (p/cm^3) and the color (blue to violet scale) is again proportional to *ln(T)*. At first sight for every dV_x bin there is approximately as much plasma moving to dawn (toward the magnetosheath) as moving to dusk (to the magnetosphere). At a closer look we may notice a slight bias. Hot-tenuous matter tends to move out, toward the magnetosheath, conversely cold-dense matter tends to move in, toward the magnetosheath. This trend is lesser in extent, more significant is that figure 21 suggests that Wind encounters the vortices at a stage of at least one roll-over, because the two classes of plasma move both, outward and inward, in almost equal proportion.

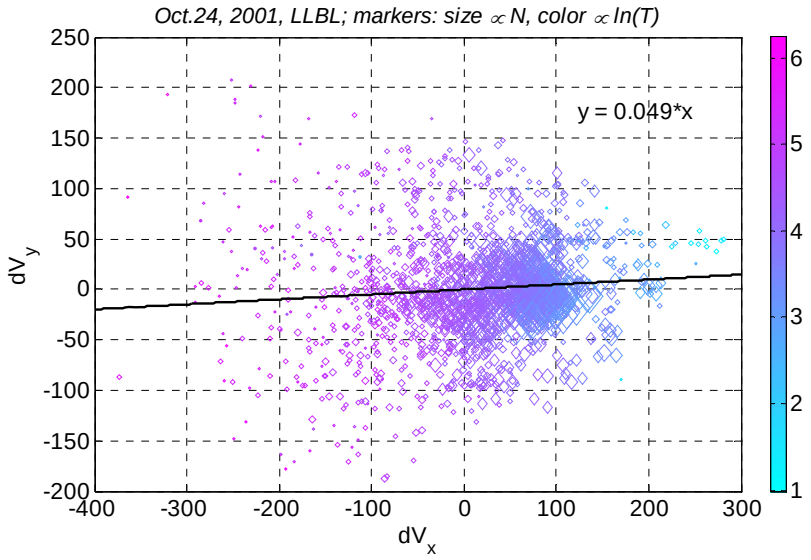

Figure 22. Scatter plot dV_y versus dV_x (in km/s) for the whole LLBL data set. The markers size is $\propto N$ (here denotes particle density) and the color is$\propto$ ln(T) (like in figure 21). The spread of positive – negative dV_y values is equiprobable at a first approximation, which can be interpreted that the vortices have done at least one turn-over. But a small bias exists, hot plasma has a slight tendency to move dawnward (toward the MS), while cold plasma shows a small preference to move toward dusk (inside the magnetosphere).

A more detailed statistical study is possible by grouping the data of the different vortices. In the last figure 23, the scatter-plots corresponds to the first five vortices observed by Wind, starting at 19 UT. Five different markers (+, ×, *o*, etc..) and colors (see the inset in the plot) identify the vortices by order of appearance in the observations. The figure format is a multivariate group representation in the fashion of a matrix, with 2×3 particular scatter-plots, in which the identity of every vortex can be distinguished. Some correlations are well defined in all five vortices, like those of dV_x-T, and dB_y-dB_x. The correlation dV_x - N is also fairly good, with the exception of the first vortex that shows more spread. In some other plots there is more disparity of behavior between vortices, like in the dB_y - N, and dV_x - dB_x correlations.

The scatter plot analysis gives decisive evidence: the observations correspond to a series of vortices. Unlike many other investigations on KH at the MP we have quoted, the case investigated is for an IMF directed mainly along +X. We suggest that the inner edge of the LLBL, where the magnetic shear is small and $\boldsymbol{k}$ perpendicular to the geomagnetic field is a right choice, become KH unstable.

Using compressible MHD theory, we have shown in section 4 that the inner edge is indeed KH unstable. Section 5 consolidated the KH vortex thesis from the experimental side. The event studied gives important clues for the evaluation of the KH stability and vortex formation of the more common Parker's spiral fields and flows.

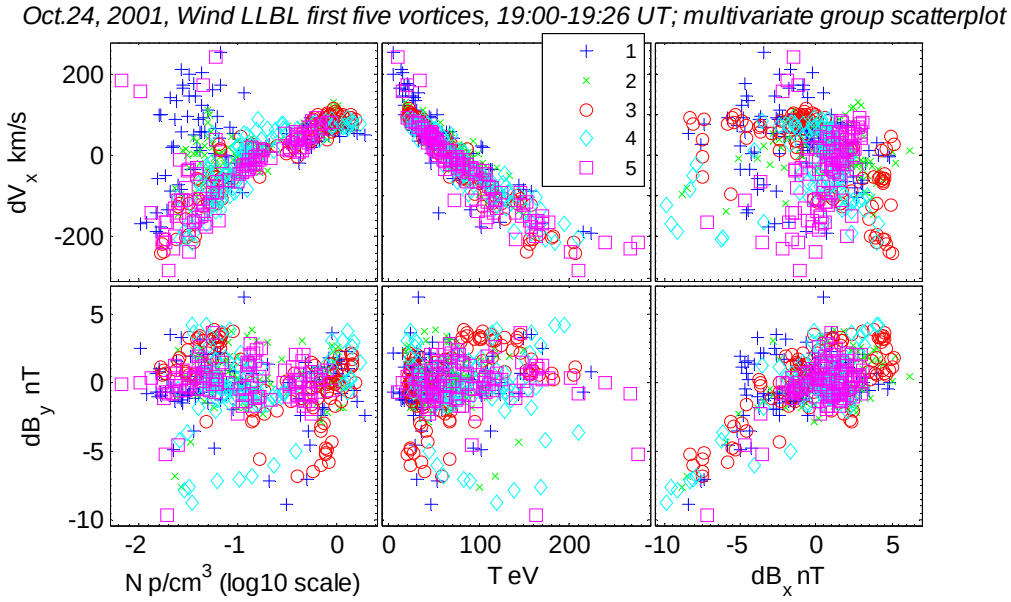

Figure 23. A multivariate scatter plot for the first five vortices observed by Wind. The markers indicate the vortices by order of appearance (see the inset). The scatter plots of pairs of quantities are shown in a matrix format. Several correlations are evident in all five vortices, like those in the scatter plots $dV_x - N$, $dV_x - T$, $dB_y - dB_x$. In other plots a different behavior between vortices is noted, as in $dB_y - N$, and dV_x - dB_x.

6. Conclusions

In the first part of this paper, the pervasive action of the KH mechanism in the solar system with a series of recent examples is described. The importance of the phenomenon for the physics of the Earth magnetosphere is emphasized, and basic concepts with equations of the MHD theory of the KH instability are outlined.

Possible objections on the limits of MHD as a plasma model lose relevance in comparison with the explanatory power of data interpretation in space plasma dynamics. The use of more sophisticated plasma theories in the context of data analysis is often an unjustified effort. It must be bear in mind that the validation of theoretical, or computational models, in space physics is inevitably indirect and limited (in contrast with the circumstances of terrestrial fluid dynamics). It is a consequence of the coherence of interpretations in a variety of observations (often qualitative rather than quantitative) and the compatibility with other theoretical models.

We then describe a set of research topics of magnetopause stability that show promise for further investigations. The instability band theory of dayside MP would benefit from further experimental work with Cluster and Themis dayside crossings under steady northward IMF conditions, and should be revisited with the help of present day global simulations. The peculiar features of pristine MP stability can be tested with data from events of sudden expansion of the magnetosphere under a drop of solar wind dynamic pressure, especially during slow solar wind periods. Magnetopause accelerations can help the start of the KH instability on the front side. The subject of the competition of KH and tearing, and its consequences, is a large area of research that in spite of important advances recorded in the literature, is still open in the directions we point out. The KH instability of the MP flanks, with the supersonic dynamics aspects on which we expatiate, and a significant case to which sections 4 – 5 are devoted, is also a rich field for further experimental and theoretical work.

In the second and last part of the paper we report a study of rolled-up vortices generated by the KH instability in the near-tail dawn flank when the IMF is pointing nearly in a radial direction (sunward). Theory models of MP at the terminator, and further downtail at Wind orbit, indicate that on October

24, 2001 the BL is Kelvin-Helmholtz unstable. This happens in spite of (*i*) the large magnetic shear across the boundary and (*ii*) the large supersonic speed (both stabilizing agents). This is possible because the Alfvén Mach number at both locales is large enough (i.e., weak magnetic tension forces), and the instability starts inside the boundary layer.

During the rise and development of the billows of this event, the collinear field is engaged as participant. Then one must face one of the two horns of a dilemma. Either the radial field component is convected and rolled-up in the vortex, or the frozen-in condition ($\boldsymbol{E}+\boldsymbol{V}\times\boldsymbol{B}=0$) breaks-down, and does not apply (or only partially). In both cases there are important consequences. In the first case there is coiling of field lines in the vortex with formation of internal current sheaths, which have been observed by Wind (as emphasized in section 5) that are prone to tearing and mass diffusion. In the second case one accepts from the start that the boundary is not a perfect shield and is porous to external mass entry.

This event differs from several other studies that reported BL vortices under strongly northward IMF orientations. This is a case of KH vortices observed under an almost radial IMF, with implicit significance for the more common Parker's spiral fields, and the problem of plasma entry in the magnetosphere.

Acknowledgements

This research was supported by CONICET grant 11220090100608 PIP 2010 - 2012 ("*La Magnetopausa en Campo Magnético Interplanetario Norte: Análisis de Datos, Teoría y Simulación de Grandes Vórtices*"). The work at University of New Hampshire was supported by NASA grant NNX08AD11G.

References

[1] Tritton D J 1988 *Physical Fluid Dynamics* (Oxford: Clarendon Press) NASA/JPL/Malin Space Science Systems site
[2] Landsat 7 WRS Path 6 Row 83, center: -33.18, -79.99.; Karman vortices, image taken 9/15/1999
[3] *Monthly Weather Review* 2006 **134** 1036
[4] *Geophysical Research Letters* 2011 Feb. 6
[5] Source http://photojournal.jpl.nasa.gov/catalog/PIA06502
[6] Masters A et al. 2010 *J. Geophys. Res.* **115** A07225 (doi:10.1029/2010JA015351)
[7] Foullon C et al. 2011 *Astrophys. J. Lett.* **729** L8; SDO/AIA, Ofman L and Thompson B J 2011 *arXiv*:1101.4249v2 [astro-ph.SR] Jan 25. NASA, SDO
[8] ed C T Russel and M G Kivelson 1995 *Introduction to Space Physics* (New York: Cambridge University Press)
[9] Sundberg T et al. 2011 *Planet. Space Sci.* doi:10.1016 /j.pss. 2011.05.008.
[10] Bochsler P et al. 2010 *Ann. Geophys.* **28** 491-7
[11] Dungey J W 1954 Pennsylvania State University, Ionosphere Research Laboratory, *Scientific Report 69*
[12] Dungey J W 1961 *Phys. Res. Lett.* **6** 47
[13] Axford W I and Hines C O 1961 *Can. J. Phys.* **39** 1433
[14] Southwood D J 1968 *Planet. Space Sci.* **16** 587
[15] Sonnerup B U O 1980 *J.Geophys. Res.* 85 2017
[16] Hones et al. 1981 *J.Geophys. Res.* **86** 814-20
[17] Ogilvie K W and R J Fitzenreiter 1989 *J. Geophys. Res.* **94** 15113
[18] Belmont G and Chanteur G 1989 *Physica Scriptae* **124** 124
[19] Miura A 1995 in *Physics of the Magnetopause*, Geophys. Monogr. Ser. **90**, 285 ed Song et al. (Washington DC: AGU)
[20] Fitzenreiter and Ogilvie 1995 in *Physics of the Magnetopause*, Geophys. Monogr. Ser. **90**, 277 ed Song et al. (Washington DC: AGU)

[21] Kivelson M G and Chen S H 1995 in *Physics of the Magnetopause*, Geophys. Monogr. Ser. **90** 257 eds Song et al. (Washington DC: AGU)
[22] Farrugia C J, Gratton F T and Torbert R B 2001 *Space Sci. Rev.* **95** 443
[23] Lepping R P and L F Burlaga 1979 *J. Geophys. Res.* **84** 7099
[24] Seon J et al 1995 *J. Geophys. Res.* **100** 907
[25] Samson J C and Rostoker G 1972 *J. Geophys. Res.* **77** 6133
[26] Kivelson M G and D J Southwood 1986 *J. Geophys. Res.* **91** 4345
[27] Miura A 1984 *J. Geophys. Res.* **89** 801
[28] Fairfield D H et al. 2000 *J. Geophys. Res.* **105** 21159
[29] Nykyri K and Otto A 2001 *Geophys. Res. Lett.* **28** 3565; Otto A and Nykyri K 2003 *Geophys. Monogr.* **133** 53 ed P T Newell and T Onsager (Washington DC: AGU)
[30] Smets R, Delcourt D, Chanteur G and Moore T E 2002 *Ann. Geophysicae* **20** 757
[31] Hasegawa H, Fujimoto M, Phan T et al. 2004 *Nature* **430** 755; Hasegawa H, Retinò A, Vaivads A et al 2009 *J. Geophys. Res.* **114** A12207 doi: 10.1029/2009JA014042
[32] Gratton F T et al. 2006 *Am. Inst. of Physics* **C P 875** Plasma and Fusion Science pp 300-3 ed. Herrera Vázquez J J E Washington DC; Gratton F T et al. 2009 *J. of Physics CS* **166** 012023 doi:10.1088/1742-6596/166/1/012023; Bilbao L 2009 *J. of Physics CS* **166** 012020 doi:10.1088/1742-6596/166/1/012020; Gratton F T et al. 2011 *J. of Physics CS* **296** 012006 doi: 10.1088/1742-6596/296/1/012006
[33] Nakamura T K M et al. 2006 *Geophys. Res. Lett.* **33** L14106 doi:10.1029/2006GL026318; Nakamura T K M et al. 2008 *J. Geophys. Res.* **113** A09204 doi:10.1029/2007JA012803
[34] Hwang K-J et al. 2011 *J. Geophys. Res.* **116** A08210 doi:10.1029/2011JA016596
[35] Fujimoto M and Terasawa T 1994 *J. Geophys. Res.* **99** 8601
[36] Otto A and Fairfield D H 2000 *J. Geophys. Res.* **105** 21175
[37] Sandholt P E, Farrugia C J, Cowley S W H *et al*. 1999 *Geophys. Res. Lett.* **26** 2833
[38] Onsager T G et al. 2001 *J. Geophys. Res*. **106** 25467
[39] Øieroset M et al. 2005 *Geophys. Res. Lett.* **32** L12S07 (doi:10.1029/2004GL021523)
[40] Gosling J T et al. 1991 *J. Geophys. Res.* **96** 14097
[41] La Belle-Hamer A L et al. 1995 *J. Geophys. Res.* **100** 11875
[42] Terasawa T *et al*. 1997 *Geophys. Res. Lett*. **24** 935
[43] Fujimoto M et al. 1998 *J. Geophys. Res.* **103** 2297; Fujimoto M et al 1998 *J. Geophys. Res.* **103** 4391
[44] Chen Q, Otto A and Lee L C 1997 *J.Geophys. Res.* **102** 151-61
[45] Fuselier S A, Petrinec S M and Trattner K J 2000 *Geophys. Res. Lett.* **27** 473
[46] Chandrasekhar S 1981 *Hydrodynamic and Hydromagnetic Stability* (Dover: Mineola); Batchelor G K 1970 *An Introduction to Fluid Dynamics* (Cambridge University Press)
[47] Gratton J and Gratton F T 1971 *Plasma Physics* **13** 567-85
[48] Kadomtsev B B 1983 *Plasma Physics* (Moscow: MIR); Pierce J R 1974 *Almost All About Waves* (Boston: MIT Press)
[49] Duhau S, Gratton F T and Gratton J 1971 *Phys. Fluids* **14** 2067-8
[50] González A G and Gratton J 1994 *J. Plasma Phys.* **51** 43; González A G and Gratton J 1994 *J. Plasma Phys.* **52** 233
[51] González A G et al. 2002 *Braz. J. Phys.* **32** 945
[52] Gratton F T et al. 2004 *Braz. J. Phys.* **34** 1804
[53] Gratton F T et al. 2004 *J. Geophys. Res.* **109** A04211 (doi:10.1029/2003JA010146)
[54] Farrugia C J et al. 1998 *J. Geophys. Res.* **103** 6703; Farrugia C J et al 1998 *Polar Cap Boundary Phenomena* ed J Moen et al (Kluwer Acad. Publ.)
[55] Gratton F T, Gratton J and González A G 1988 *Plasma Phys. Controlled Fusion* **30** 435
[56] Gnavi G et al. 2009 *J. of Physics C. S.* **166** 012022 (doi:10.1088/1742-6596/166/1/012022)
[57] Landau L D 1944 *Dokl. Akad. Nauk. SSSR* **44** 151
[58] Farrugia C J et al. 2003 *Adv. Space Res.* **31** 1105

[59] Southwood D J 1974 *Planet.Space Sci*. **22** 483; Kivelson M G and Southwood D J 1986 *J.Geophys.Res.* **91** 4345-51
[60] Contin J E, Gratton F T and Farrugia C J 2003 *J Geophys. Res.* **108** 1227
[61] Eastman T E, Fuselier S A and Gosling J T 1996 *J. Geophys. Res.* **101** 49
[62] Gratton F T, Farrugia C J and Cowley S W 1996 *J. Geophys. Res.* **101** 4929
[63] Gratton F T et al. 2003 *Planetary and Space Science* **51** 769-83
[64] Furth H P, J Killeen and M N Rosenbluth 1963 *Phys. of Fluids* **6** 495
[65] Ofman L 1991 *Phys. Fluids* **B3** 1364; Ofman L 1992 *Phys. Fluids* **B4** 2751; Einaudi G 1999 *Plasma Phys.Control. Fusion* **41** A293
[66] Fuselier S A, Elphic R C and Gosling J T 1999 *J. Geophys. Res.* **104** 4515
[67] Farrugia C J et al 2000 *J. Geophys. Res.* **105** 7639
[68] Gosling et al. 1991 *J. Geophys. Res.* **96** 14097
[69] Phan T D, Lin R P, Fuselier S A and Fujimoto M 2000 *J. Geophys. Res.* **105** 5497
[70] Øieroset et al. 2002 *Earth's Low-Latitude Boundary Layer* **133** ed P T Newell and T G Onsager (Washington DC: AGU) p 253; Øieroset M et al, 2008 *Geophys. Res. Lett.* **35** L17811 (doi:10.1029/2008GL033661)
[71] Li W et al. 2005 *Geophys. Res. Lett.* **32** L12S08 (doi:10.1029/2004GL021524)
[72] Bender L *Procesos disipativos rápidos en magnetohidrodinámica* 1997 Physics PhD Thesis, Facultad de Ciencias Exactas y Naturales, Universidad de Buenos Aires, Biblioteca FCEyN: Tesis n 2957
[73] Bender L et al. 1998 *Anales AFA* **8** ed R. Gratton et al. (Tandil: ISSN 0327-358X)
[74] Gratton F T and Krasnopolsky R 1994 *Proc. The Solar Wind-Magnetosphere System* ed H. K. Biernat et al. (Vienna: Austrian Academy of Sciences ISBN 3-7001-2127-X) pp 343-57
[75] Gnavi G, Gratton F T and Farrugia C J 2000 *J. Geophy. Res.* **105** A9 20973-87; Gnavi G, Farrugia C J and Gratton F T 2000 *Proc. ICPP 2000* vol 3 (Quebec) p 1060; Gnavi G, Farrugia C J and Gratton F T 2004 *Braz. J. Phys.* **34** 1797-803
[76] Farrugia C J et al. 2004 *J. Geophys. Res.* **109** 1-16; Farrugia C J et al. 2005 *Annales Geophysicae* **23** 1317-33
[77] Weiss N O 1966 *Proc. R. Soc. Lond.* A **293** 310-28 (doi:10.1098/rspa.1966.0173)
[78] Farrugia C J et al. 2008 *J. Geophys. Res.* **113** A03208 (doi:10.1029/2007JA012800)
[79] Farrugia C J and Gratton F T 2009 *J. Atmos. Solar-Terr. Phys* (doi:10.1016/j.jastp.2009.10.008)
[80] Foullon C et al 2008 *J. Geophys. Res.* **113** A11203 (doi:10.1029/2008JA013175); Foullon C et al 2009 *J. Geophys. Res.* **114** A10201 (doi:10.1029/2009JA014444); Foullon C et al 2010 *J. Geophys. Res.* **115** A09203 (doi:10.1029/2009JA015189)
[81] Paschman G S et al. 2005 *Ann. Geophys*. **23** 1481
[82] Farrugia C J et al. 2010 *J. Geophys. Res.* **115** A08227 (doi:10.1029/2009JA015128)
[83] Farrugia C J et al. 2007 *Ann. Geophys.* **25** 1-15
[84] Spreiter J R and Rizzi A W 1974 *Acta Astron.* **1** 15–35
[85] Chen S H et al. 1993 *J. Geophys. Res.* **98** 5727
[86] Takagi K C et al. 2006 *J. Geophys. Res.* **111** A08202 (doi:10.1029/2006JA011631); Hasegawa H et al. 2006 *J. Geophys. Res.* **111** A09203 (doi:10.1029/2006JA011728)

Erratum

An earlier version of this paper was published in error, which did not include some updates to the references. The updated references can be found below.

[4] Van Haren H and Gostiaux L 2010 *Geophys. Res. Letters* **37** L03605
[32] Gratton F T et al 2006 *AIP Conference Proceedings* **875** 300-3; Gratton F T et al. 2009 *J. of Physics CS* **166** 012023 doi:10.1088/1742-6596/166/1/012023; Bilbao L 2009 *J. of Physics CS* **166** 012020 doi:10.1088/1742-6596/166/1/012020; Gratton F T et al. 2011 *J. of Physics CS* **296** 012006 doi: 10.1088/1742-6596/296/1/012006
[75] Gnavi G, Gratton F T and Farrugia C J 2000 *J. Geophys. Res.* **105** 20973-87; Gnavi G, Farrugia C J and Gratton F T 2000 *Proc. ICPP* 2000 vol 3 (Quebec) p 1060; Gnavi G, Farrugia C J and Gratton F T 2004 *Braz. J. Phys.* **34** 1797-803